Geochemistry Geophysics Geosystems G3

Article
Volume 12, Number 3
31 March 2011
Q0AE02, doi:10.1029/2010GC003402
ISSN: 1525-2027

Published by AGU and the Geochemical Society

Crustal thickness anomalies in the North Atlantic Ocean basin from gravity analysis

Tingting Wang
Institute of Theoretical and Applied Geophysics, School of Earth and Space Sciences, Peking University, Beijing 100871, China

Jian Lin and Brian Tucholke
Department of Geology and Geophysics, Woods Hole Oceanographic Institution, Woods Hole, Massachusetts 02543, USA (jlin@whoi.edu)

Yongshun John Chen
Institute of Theoretical and Applied Geophysics, School of Earth and Space Sciences, Peking University, Beijing 100871, China

[1] Gravity-derived crustal thickness models were calculated for the North Atlantic Ocean between 76°N and the Chain Fracture Zone and calibrated using seismically determined crustal thickness. About 7% of the ocean crust is <4 km thick (designated as thin crust), and 58% is 4–7 km thick (normal crust); the remaining 35% is >7 km thick and is interpreted to have been affected by excess magmatism. Thin crust probably reflects reduced melt production from relatively cold or refractory mantle at scales of up to hundreds of kilometers along the spreading axis. By far the most prominent thick crust anomaly is associated with Iceland and adjacent areas, which accounts for 57% of total crustal volume in excess of 7 km. Much smaller anomalies include the Azores (8%), Cape Verde Islands (6%), Canary Islands (5%), Madeira (<4%), and New England–Great Meteor Seamount chain (2%), all of which appear to be associated with hot spots. Hot spot–related crustal thickening is largely intermittent, suggesting that melt production is episodic on time scales of tens of millions of years. Thickened crust shows both symmetrical and asymmetrical patterns about the Mid-Atlantic Ridge (MAR) axis, reflecting whether melt anomalies were or were not centered on the MAR axis, respectively. Thickened crust at the Bermuda and Cape Verde rises appears to have been formed by isolated melt anomalies over periods of only ~20–25 Myr. Crustal thickness anomalies on the African plate generally are larger than those on the North American plate; this most likely results from slower absolute plate speed of the African plate over relatively fixed hot spots.

Components: 14,100 words, 14 figures, 4 tables.

Keywords: crustal thickness; gravity; hot spot; North Atlantic.

Index Terms: 8137 Tectonophysics: Hotspots, large igneous provinces, and flood basalt volcanism; 8122 Tectonophysics: Dynamics: gravity and tectonics; 3035 Marine Geology and Geophysics: Midocean ridge processes.

Received 18 October 2010; **Revised** 9 February 2011; **Accepted** 18 February 2011; **Published** 31 March 2011.

Wang, T., J. Lin, B. Tucholke, and Y. J. Chen (2011), Crustal thickness anomalies in the North Atlantic Ocean basin from gravity analysis, *Geochem. Geophys. Geosyst.*, *12*, Q0AE02, doi:10.1029/2010GC003402.

Theme: From the Mantle to the Ocean: Life, Energy, and Material Cycles at Slow Spreading Ridges
Guest Editors: C. Devey, N. Dublilier, J. Lin, N. Le Bris, and D. Connelly

1. Introduction

[2] Crustal accretion at the northern Mid-Atlantic Ridge (MAR) (Figure 1a) is generally considered to be magma-limited because of the slow spreading rate of the ridge (Figure 1b). This results in a relatively cold thermal structure with a strong lithosphere, leading to a deep axial rift valley and rugged terrain created by large and widely spaced normal faults at the ridge axis [*Macdonald*, 1982; *Chen and Morgan*, 1990; *Shaw and Lin*, 1993]. Mantle upwelling and crustal accretion at slow spreading ridges is believed to be a 3-D process that gives rise to significant segment-scale variations in crustal thickness, with enhanced magma supply toward segment centers and less magma at segment ends [*Kuo and Forsyth*, 1988; *Lin et al.*, 1990; *Minshull et al.*, 1991; *Chen*, 1992; *Lin and Phipps Morgan*, 1992; *Tolstoy et al.*, 1993; *Canales et al.*, 2000; *Hooft et al.*, 2000]. Thus, overall, we expect rougher topography, larger relief, and thinner and less uniform crust at slow spreading ridges than at fast spreading ridges.

[3] Major exceptions to the magma-limited character of the MAR are hot spot–influenced regions, with Iceland and the Azores being the most prominent examples (Figure 1a). These areas are characterized by elevated topography [*Vogt*, 1976; *Schilling*, 1985], pronounced negative Bouguer anomaly or mantle Bouguer anomaly (MBA) [*Thibaud et al.*, 1998; *Gente et al.*, 2003; *Fedorova et al.*, 2005] and enriched mantle chemical compositions [*Schilling*, 1973, 1975; *Schilling et al.*, 1983; *Yu et al.*, 1997; *Dosso et al.*, 1999]. These anomalies have been attributed to hot spots that generate enormous volumes of basaltic magma on or near the ridge axis [*Schilling*, 1991; *Ito et al.*, 1996; *Cannat et al.*, 1999]. Other, volumetrically less important anomalies have been created by the New England, Madeira, Canary, and Cape Verde hot spots. Some features, notably the Bermuda Rise, are not so clearly related to hot spot activity.

[4] While many gravity and seismic investigations have been conducted locally in the North Atlantic, few studies have evaluated gravity anomalies and crustal thickness variations throughout the entire region. *Crosby and McKenzie* [2009] examined the global relationship between residual topography and gravity, and they estimated the volume and buoyancy flux of several plume swells based on residual topography. Unlike the individual examples discussed by *Crosby and McKenzie* [2009], we here use geophysical data to calculate model crustal thickness throughout the entire North Atlantic from the Chain Fracture Zone in the equatorial Atlantic to 76°N, and we thereby investigate the complete regional spatial distribution and volumes of potential melt anomalies. *Louden et al.* [2004] calculated isostatic crustal thickness for the northern North Atlantic region (30°–70°N); our results show generally similar patterns in this region but differ in detail because we used different methodology (see section 5.4).

[5] Here we use combinations of seafloor bathymetry (Figure 1a) [*Smith and Sandwell*, 1997], crustal age data (Figure 1c) [*Müller et al.*, 2008], satellite-derived free-air gravity (Figure 1d) [*Sandwell and Smith*, 2009], and sediment thickness (Figure 1e) [*Divins*, 2009] to calculate the residual mantle Bouguer anomaly (RMBA), which we invert to obtain model crustal thickness. Using this result, we divide the modeled crustal thickness into categories of thin (<4 km), normal (4–7 km) and thick (>7 km) crust, and we discuss the distribution and likely origins of these variations.

2. Geological Background

[6] The North Atlantic Ocean basin contains the oldest in situ oceanic crust on the Earth, excepting a small area in the western Pacific Ocean. Seafloor spreading in the central North Atlantic Ocean started in the Middle Jurassic (~180 Ma) when the

Figure 1. (a) Bathymetry of the North Atlantic Ocean [*Smith and Sandwell*, 1997] in Albers Conic Equal-Area projection. Features marked are Azores-Biscay Rise (ABR), Atlantis seamounts (ATS), Azores, Baffin Bay (BB), Bermuda Rise (BR), Charlie Gibbs Fracture Zone (CGFZ), Charcot seamounts (CHS), Canary Islands (CI), Ceara Rise (CR), Corner seamounts (CS), Cape Verde Islands (CVI), Davis Strait (DS), East Thulean Rise (ETR), Fogo seamounts (FGS), Fifteen Twenty Fracture Zone (FTFZ), Great Meteor seamounts (GMS), Hayes Fracture Zone (HFZ), Horseshoe seamounts (HS), Iceland, J Anomaly Ridge (JAR), Jan Mayen Fracture Zone (JMFZ), Kane Fracture Zone (KFZ), Kings Trough (KT), Milne seamounts (MS), Madeira-Tore Rise (MTR), New England seamounts (NES), Newfoundland seamounts (NFS), Southeast Newfoundland Ridge (SENR), Sierra Leone Rise (SLR), Vema Fracture Zone (VFZ), and West Thulean Rise (WTR). (b) Map of spreading half rate in the North Atlantic Ocean [*Müller et al.*, 2008]. (c) Map of crustal age in the North Atlantic Ocean [*Müller et al.*, 2008]. (d) Map of satellite-derived free air anomaly (FAA) for the North Atlantic Ocean [*Sandwell and Smith*, 2009]. (e) Map of sediment thickness in the North Atlantic Ocean [*Divins*, 2009].

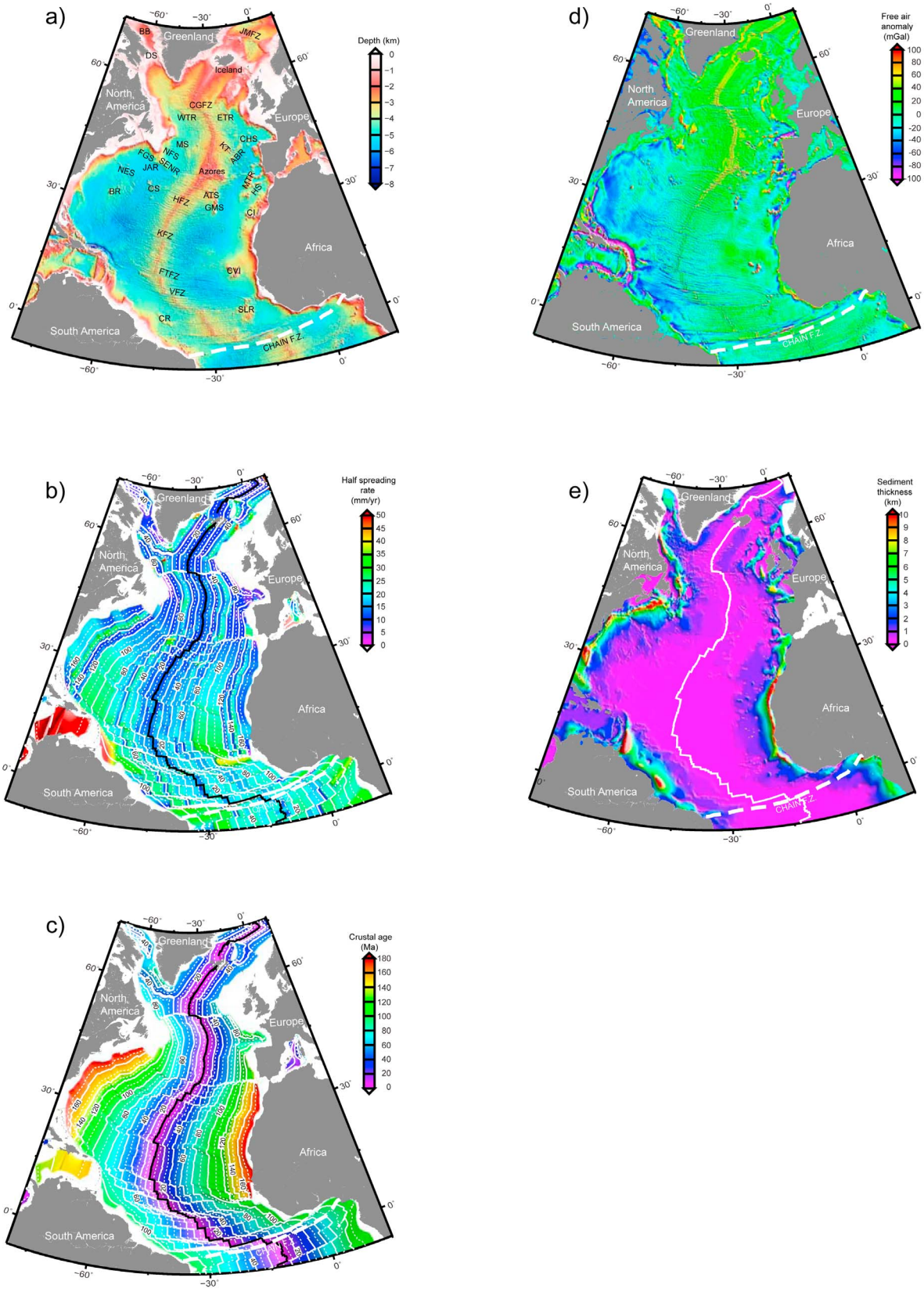
a)
Depth (km)
0
−1
−2
−3
−4
−5
−6
−7
−8
Greenland
Iceland
North America
Europe
Africa
South America
BB
DS
JMFZ
CGFZ
WTR
ETR
CHS
MS
KT
ABR
NFS
FGS
SENR
JAR
NES
Azores
MTR
KS
BR
CS
HFZ
ATS
GMS
CI
KFZ
FTFZ
CVI
VFZ
SLR
CR
CHAIN F.Z.
b)
Half spreading rate (mm/yr)
50
45
40
35
30
25
20
15
10
5
0
c)
Crustal age (Ma)
180
160
140
120
100
80
60
40
20
0
d)
Free air anomaly (mGal)
100
80
60
40
20
0
-20
-40
-60
-80
-100
e)
Sediment thickness (km)
10
9
8
7
6
5
4
3
2
1
0

Figure 1

North American plate separated from the African plate (Figure 1c) [*Klitgord and Schouten*, 1986] (the timescales of *Cande and Kent* [1995] and *Gradstein et al.* [1994] are used in this study). Farther north, the Newfoundland-Iberia margins rifted apart in Late Jurassic to Early Cretaceous and seafloor spreading there started no later than about 112 Ma [*Tucholke et al.*, 2007]. During the Late Cretaceous, rifting moved farther north into Rockall Trough and the Labrador Sea [*Srivastava and Tapscott*, 1986], although rifting in Rockall Trough probably did not reach the seafloor spreading stage [*Klitgord and Schouten*, 1986]. The time of initial seafloor spreading in the Labrador Sea and Baffin Bay has been debated, with interpretations varying from 80 Ma to 62 Ma (chrons 33 to 27) [*Roest and Srivastava*, 1989; *Chian and Louden*, 1994; *Chalmers and Laursen*, 1995]. A significant change in spreading direction took place there at 59–56 Ma (chron 25–24), at the same time that seafloor spreading initiated in the Norwegian-Greenland Sea [*Klitgord and Schouten*, 1986; *Srivastava and Tapscott*, 1986]. Spreading in the Labrador Sea and Baffin Bay stopped at 35 Ma (chron 13).

[7] We expect three primary geological causes for variations in oceanic crustal thickness: (1) the fertility of upwelling mantle at the ridge axis, (2) spreading/upwelling rate, and (3) hot spots. Oceanic crust is formed along mid-ocean ridges where upwelling mantle undergoes decompression melting. The amount of melting and crustal accretion is affected by variations in mantle composition, water content, and thermal state [e.g., *Langmuir et al.*, 1992; *Bonatti et al.*, 2003]. Because these variations occur beneath the ridge axis, they produce axial-symmetric changes in crustal thickness.

[8] Studies have shown that strongly thinned crust is produced under very slow spreading rate (e.g., half rate of <7.5–10 mm yr^{-1}) [*Reid and Jackson*, 1981; *Bown and White*, 1994; *White et al.*, 2001], and this is an axial-symmetric effect along the ridge axis. Spreading half rates in the North Atlantic (Figure 1b) generally have varied from 7 to 25 mm yr^{-1} with an average rate of about 16 mm yr^{-1} [*Müller et al.*, 2008]. Overall, spreading rate in the south is higher than that in the north due to greater distance from the poles of rotation of North Atlantic opening. The central Atlantic spread at ~19 mm yr^{-1} from 170 Ma until around 155 Ma (chron M25), when a sharp increase to 25 mm yr^{-1} occurred. The spreading half rate decreased at ~145 Ma (chron M19) and was less than 10 mm yr^{-1} around 130 Ma (chron M10). The spreading rate in the central Atlantic averaged 24 mm yr^{-1} throughout the Cretaceous Magnetic Quiet Zone (~120 to 84 Ma, chrons M0 to 34), but it could have varied significantly from this value because there are no chrons to constrain the rates during this period. Following ~84 Ma (chron 34), the spreading rate remained low (below ~18 mm yr^{-1}) except for an increase to about 22 mm yr^{-1} at 60–50 Ma (chron 26–22). At present, the Atlantic is spreading at a half rate of 12 to 13 mm yr^{-1}.

[9] On-ridge-axis and near-ridge-axis hot spots generally produce crustal thickness patterns that are symmetrical about the axis, while intraplate hot spots generate asymmetrical patterns. The magnitude of crustal thickening is influenced both by the rate at which excess melt is introduced and by the speed of the plate moving over the hot spot, with slower motion producing a thicker crust. The African plate has been moving with a much slower speed than the North American plate [*Müller et al.*, 1993], as indicated for example by calculated hot spot tracks [*Duncan*, 1984; *Müller et al.*, 1993]. As we will discuss, the difference in plate speed introduces different degrees of crustal thickening in the two plates.

3. Data and Analysis

3.1. Bathymetry and Free-Air Gravity Anomaly

[10] Bathymetric data used in this study are from the Global Topography data set (V12.1) [*Smith and Sandwell*, 1997], derived from a combination of ship track measurements and satellite altimetry data. We extracted the North Atlantic bathymetric data from a global 1 min grid (Figure 1a). In general, we found that bathymetry extracted from this global data set is in good agreement with that determined from shipboard measurements in specific areas (see Figure S3).[1]

[11] We also used Geosat and ERS-1 satellite-derived free-air anomaly (FAA) gravity data (Figure 1d) [*Sandwell and Smith*, 2009] in a 1 min grid database. Previous studies have shown that satellite-derived free-air anomalies are close to shipboard measurements for wavelengths longer than 25–30 km [*Neumann et al.*, 1993; *Marks*, 1996].

3.2. Sediment Thickness

[12] To correct for gravitational and loading effects of sediments, we extracted sediment thickness data

[1] Auxiliary materials are available in the HTML. doi:10.1029/2010GC003402.

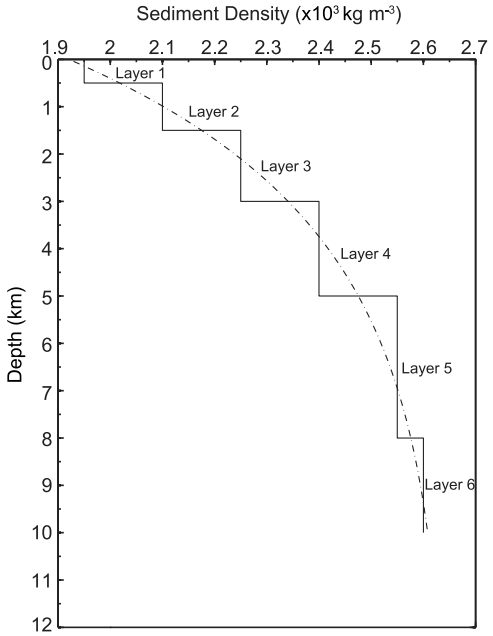

Figure 2. Exponential density-depth curve (dotted dashed line) following *Cowie and Karner* [1990, Figure 2b]. The solid line shows stepwise density-depth ranges that we used to calculate sediment corrections.

(Figure 1e) from the 5 min global database of *Divins* [2009]. In most of the North Atlantic away from continental margins the sediment thickness is less than 1 km. Thicker sediments occur primarily along the continental margins and can exceed 10 km on the older margins. When comparing sediment thickness from the global data set with local surveys we find that there is generally a reasonable fit, although differences in details do exist (see Figure S3). Such discrepancies may introduce uncertainties in calculated gravity anomalies, especially for margins with great sediment thickness.

[13] Sediment density increases with depth as sediment compacts, and *Cowie and Karner* [1990] described this relationship as an exponential function (Figure 2) with parameters varying with different lithologies. The exponential function fits well-log data in several sediment basins, but there are significant uncertainties in density versus depth for depths greater than 5 km. In our gravity calculations we used the *Cowie and Karner* [1990] density-depth function, dividing the sedimentary section into 6 layers with stepwise density values (Figure 2).

3.3. Crustal Age

[14] Global crustal age data in a 6 min grid (Figure 1c) from *Müller et al.* [2008] were used when calculating lithosphere cooling effects, as discussed in section 3.4. Age errors are a function of errors in magnetic anomaly identification and they also depend on distances between grid elements and the nearest magnetic anomaly identification [*Müller et al.*, 2008]. Overall, age errors do not exceed 3 Myr for most of our study area, although larger errors can be associated with narrow zones associated with offsets at fracture zones and other sharp age discontinuities. In general, age errors of ca. 3 Myr have no appreciable effect on lithosphere thermal corrections; this is especially true in older crust where the difference in thermal correction is relatively small for moderate age differences.

3.4. Thermal Correction

[15] We calculated the gravitational effect of lithospheric cooling, i.e., the thermal correction, using a 3-D thermal model. The thermal structure was calculated from 0 to 100 km depth using the age grid (Figure 1c) and a simple 1-D plate cooling model [*Turcotte and Schubert*, 2002] with temperatures of $T_s = 0°C$ at the surface and $T_m = 1350°C$ at 100 km depth (Table 1). The thermal structure was then converted into a 3-D density grid using the thermal expansion equation, $\Delta\rho = (T_0 - T)\ \alpha\ \rho_0$, where T_0 and ρ_0 are reference temperature and density, respectively. We used $T_0 = 1350°C$ and $\rho_0 = 3.3 \times 10^3$ kg m^{-3}.

Table 1. Parameters Used in Calculations

Parameter	Definition	Value
ρ_w	Water density, kg m^{-3}	1.03×10^3
ρ_c	Crust density, kg m^{-3}	2.7×10^3
ρ_m	Mantle density, kg m^{-3}	3.3×10^3
H	Plate thickness, km	100
α	Volumetric coefficient of thermal expansion, °C^{-1}	3×10^{-5}
T_s	Temperature at the surface of the plate, °C	0
T_m	Temperature at the bottom of the plate, °C	1350
ρ_0	Reference density, kg m^{-3}	3.3×10^3
T_0	Reference temperature, °C	1350

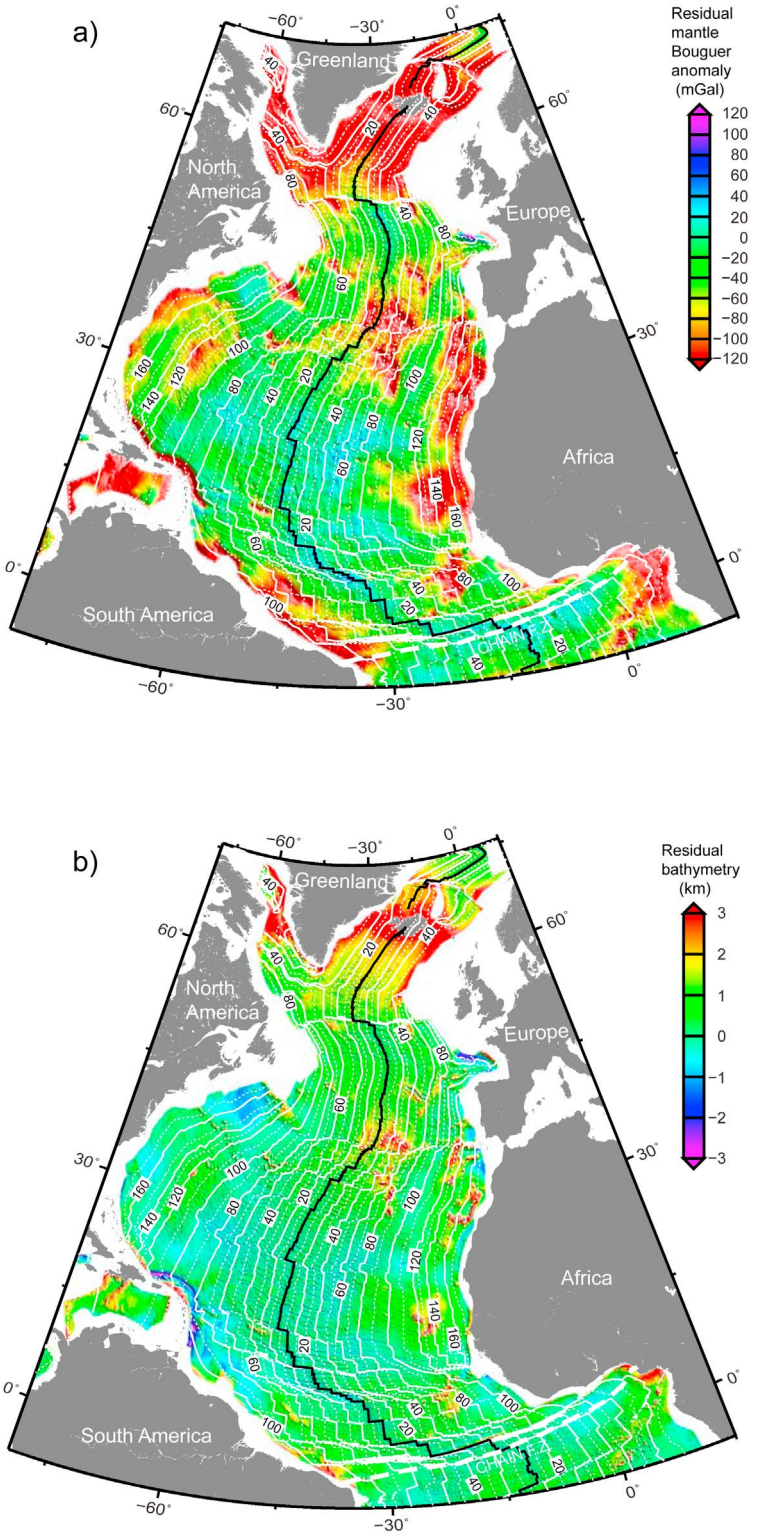

Figure 3. (a) Map of calculated residual mantle Bouguer anomaly (RMBA) for the North Atlantic. Crustal age isochrons are from *Müller et al.* [2008]. (b) Map of calculated residual bathymetry anomaly.

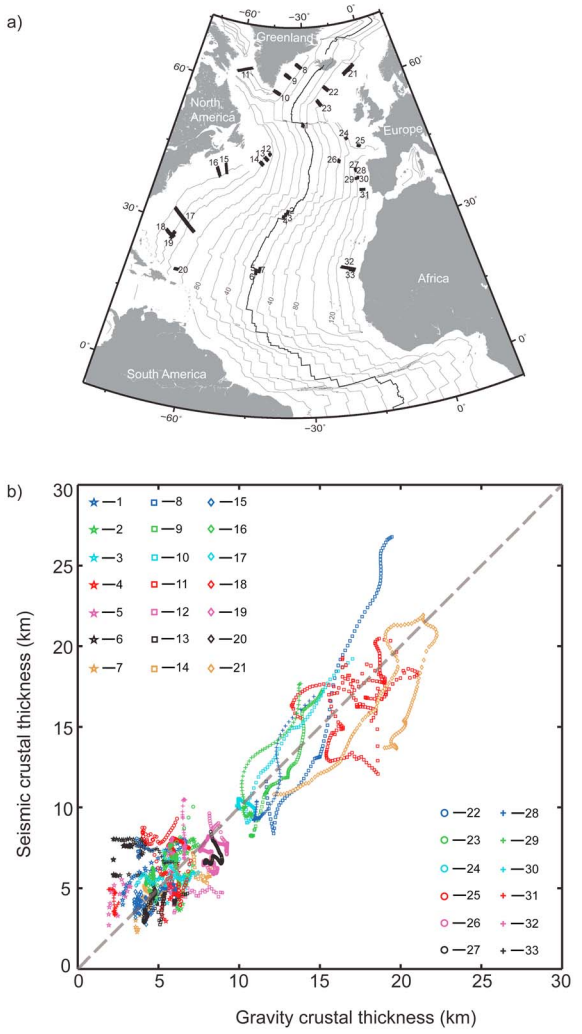

Figure 4. (a) Locations of seismic refraction profiles used for comparison of gravity-derived and seismically determined crustal thickness in Figure 4b. See Figure S3 for comparisons within individual seismic profiles. (b) Comparison of gravity-derived crustal thickness (Figure 5) with seismically determined crustal thickness from 33 seismic refraction profiles in the North Atlantic Ocean. Each point corresponds to a sample every 2 km along the seismic profile. Symbols are identified with profile numbers shown in Figure 4a.

[16] In our thermal model we ignored the effect of near-ridge-axis hydrothermal cooling and thus the resultant temperature for the ridge axis may be hotter than reality. Using such hotter mantle temperature in the thermal model can lead to thinner calculated crustal thickness. However, this effect is limited to within ~10–20 km of the ridge axis and it therefore does not affect the main conclusions of this study.

3.5. Residual Mantle Bouguer Anomaly

[17] We used the spectrum method of *Parker* [1972] to first calculate the mantle Bouguer anomaly by subtracting from the free-air anomaly the predicted attractions of the water-sediment, sediment-crust, and crust-mantle interfaces, assuming a constant reference crustal thickness of 7 km. Densities of water, crust, and mantle were assumed to be 1.03, 2.7, and 3.3×10^3 kg m^{-3}, respectively. Residual mantle Bouguer anomaly (RMBA) (Figure 3a) was then calculated by removing from the mantle Bouguer anomaly the gravitational effect of lithospheric cooling (Figure S1).[1] The parameters that we used in the calculation are summarized in Table 1.

[18] We performed a series of calculations to test the sensitivity of the results to the assumed model parameters. We found that as long as the density contrast between water and mantle remains the same, changing the value for crustal density has no detectable effect on the RMBA signal.

3.6. Crustal Thickness

[19] Both crust and mantle density variations contribute to the RMBA [*Magde et al.*, 1995; *Canales et al.*, 2002]. In this paper we investigated end-member models in which the RMBA signal is assumed to be caused only by crustal thickness variations.

[20] We calculated a series of crustal thickness models, corresponding to assumed crustal densities of 2.7 to 3.0×10^3 kg m^{-3} in 0.05×10^3 kg m^{-3} steps, while fixing mantle density at 3.3×10^3 kg m^{-3}. All calculations were done by downward continuing the RMBA to a constant depth using the method of *Kuo and Forsyth* [1988]. There is a trade-off between the calculated relative crustal thickness and the crust-mantle density contrast at the Moho. For the same RMBA, a larger density crust-mantle density contrast will produce smaller lateral crustal thickness variation.

[21] We tested downward continuation depths at 5, 6, 7, 8, 9, 10, 11 km, respectively. It turned out that the results from different downward continuation depths have no appreciable difference after shifting to fit to the seismic determined crustal thickness (see section 3.7). In this study we presented the results from downward continuation depths of 10 km.

[22] We filtered the RMBA data before downward continuation. A cosine taper was performed at a wavelength range from 25 km to 135 km. Signals with wavelengths less than 25 km were cut off and

Table 2. Sensitivity of Model Results to Assumed Crustal Density

Assumed Crustal Density (kg m^{-3})	Best Fitting Slope[a]	RMS (km)[b]
2.7	0.88	2.07
2.75	0.80	2.25
2.8	0.73	2.55
2.85	0.66	3.03
2.9	0.59	3.71
2.95	0.51	4.67
3.0	0.44	5.99

[a]Fit to the data using the relationship: seismic thickness $T_{seism} = T_c + R \times T_{grav}$, where T_c is the y intercept, R is the best fitting slope, and T_{grav} is gravity-derived thickness.
[b]Root mean square for the difference between gravity-derived and seismically determined crustal thickness.

signals with wavelengths larger than 135 km were kept in their entirety.

3.7. Comparison With Seismic Studies

[23] To calibrate our gravity-derived crustal thickness model, we compared our results to crustal thickness determined in 33 representative seismic refraction profiles in the North Atlantic (Figure 4a and Figure S3). For each model of different crustal density we shifted the gravity-derived crustal thickness values as a whole to obtain minimum root mean square (RMS) of the difference between gravity-derived and seismically determined crustal thickness. We also calculated the best fitting slope between gravity-derived and seismically determined crustal thickness for each of the models (Table 2). We found that the model with *average* crustal density of 2.7×10^3 kg m^{-3} has both the smallest RMS and best fitting slope close to 1 (Table 2), and we therefore consider this to be the best model. The resulting crustal thickness map is shown in Figure 5.

[24] Figure 4b summarizes the relationship between gravity-derived and seismically determined crustal thickness for the 33 seismic refraction profiles (see also Figure S3) for our best fitting model with crustal density of 2.7×10^3 kg m^{-3}. The gravity and

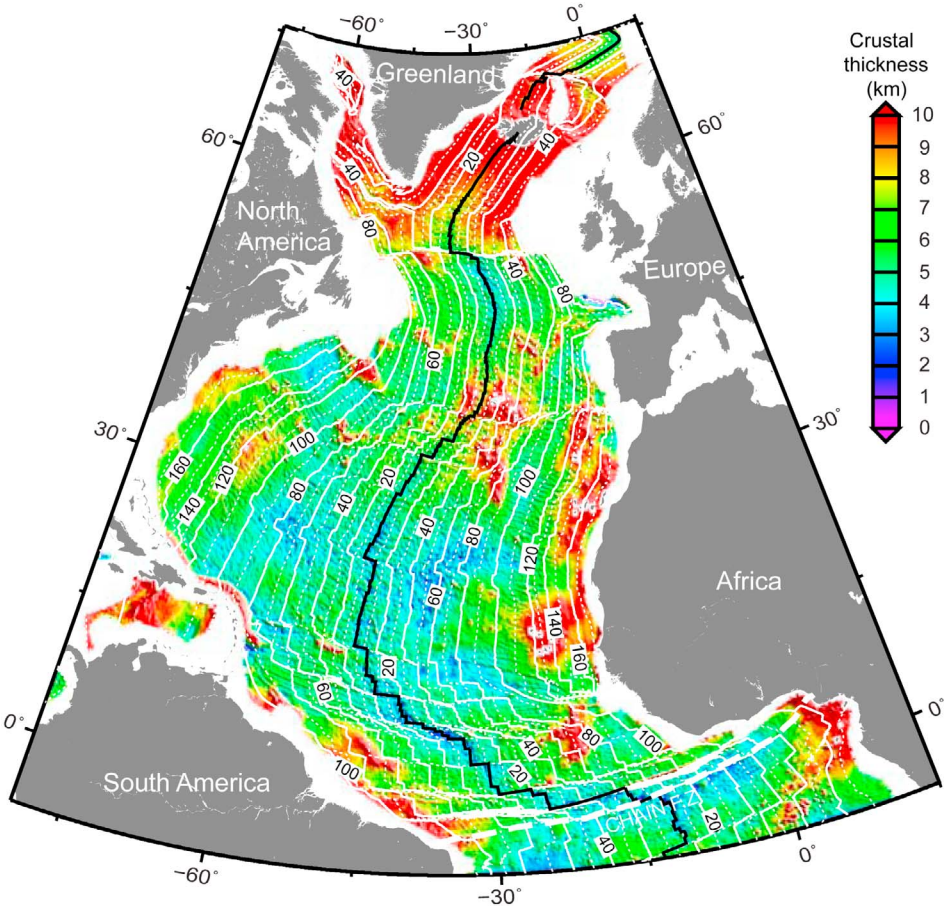

Figure 5. Map of crustal thickness based on the assumption that all RMBA variations are caused by crustal thickness variations. The result shown is the best fitting model based on sensitivity tests; it corresponds to an average crustal density of 2.7×10^3 kg m^{-3} and mantle density of 3.3×10^3 kg m^{-3}.

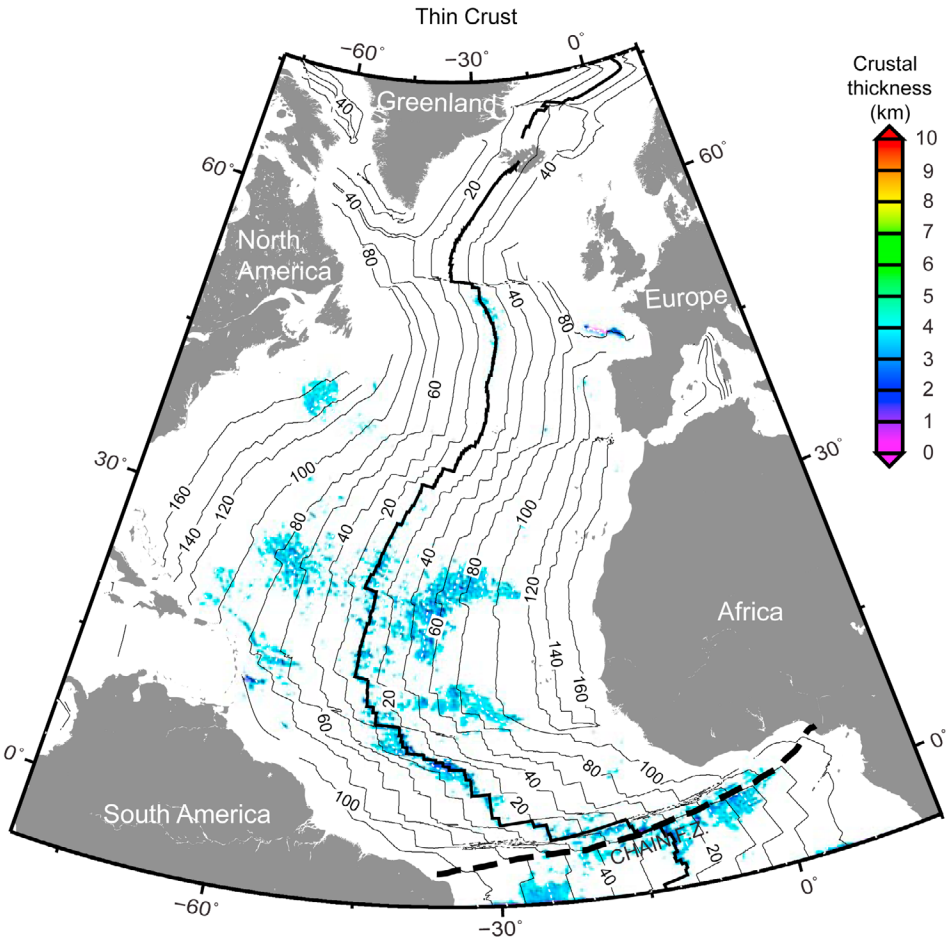

Figure 6. Map of modeled crustal thickness showing areas of thin crust (<4 km).

seismic results broadly agree in defining areas of thin versus thick crust. However, the gravity-derived and seismically determined crustal thickness values rarely correlate closely along any given profile. The causes of these differences can arise from a number of effects. In particular, lateral mantle and crustal density variations not considered in our gravity models may account for much of the variation. There are also significant resolution differences between our bathymetry and sediment thickness data and the higher-resolution data of seismic surveys that contribute to the variation. Considering these factors, it is clear that our model results do not necessarily predict local (less than a few tens of kilometers) crustal thickness accurately. However, they do provide important information about variations at subregional to regional scales, and we use our results in this context.

3.8. Residual Bathymetry Anomaly

[25] We define residual bathymetry anomaly (RBA) (Figure 3b) as the observed seafloor bathymetry minus the predicted effects of plate cooling after correcting for sediment loading. The sediment correction is applied assuming Airy compensation of the sediment load $\Delta Z = h_s\ (\rho_m - \rho_s)/(\rho_m - \rho_w)$, where ΔZ is the correction to bathymetry, h_s is sediment thickness, and ρ_m, ρ_s and ρ_w are densities of the mantle, sediment, and water, respectively. Depth-dependent sediment densities (Figure 2) and mantle and water densities are the same as used in gravitational calculations (Table 1). The predicted effect of plate cooling is calculated using the same plate-cooling model [*Turcotte and Schubert*, 2002] as for the RMBA calculation.

4. Results

[26] Based on our model crustal thickness results we partition the oceanic crust in the North Atlantic between the Chain Fracture Zone and 76°N into three categories: (1) thin crust (<4 km; Figure 6), (2) "normal crust" (4–7 km; Figure 7), and (3) thickened crust (>7 km; Figure 8). The Caribbean

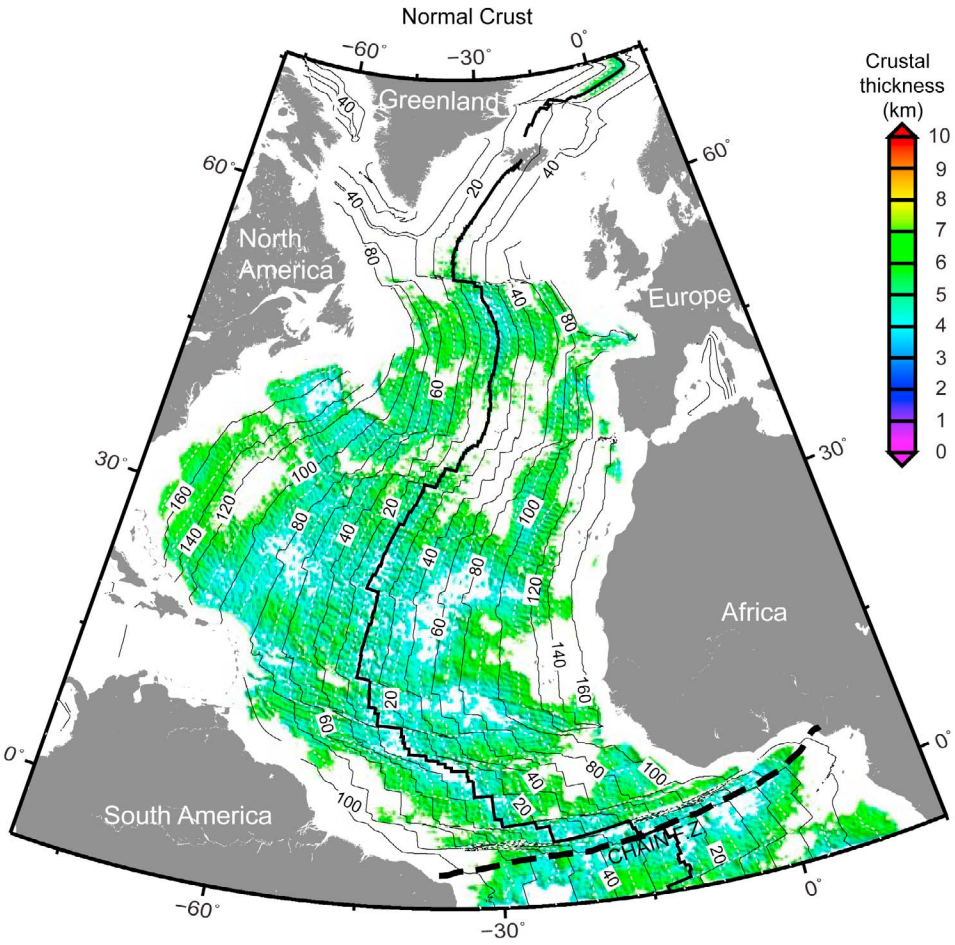

Figure 7. Map of modeled crustal thickness for areas of normal crust (4–7 km).

is not included. Within the North Atlantic region, we calculated the area of oceanic crust in each of the above three categories (Figures 9a and 10a) and we also calculated the crustal volume for each category (Figures 9b and 10b). These results and comparison with the total volume of North Atlantic oceanic crust are summarized in Table 3.

4.1. Thin Crust

[27] Major regions of modeled thin crust (Figure 6) in the North Atlantic are observed between 20°N and 28°N, extending from crustal ages of about 40 Ma out to about 110 Ma. To the north, a small but prominent area of thin crust appears next to the Nova Scotia margin. West-southwest of the Cape Verde Islands, a zone of thin crust lying at 60–100 Ma is found between the Fifteen Twenty Fracture Zone and Vema Fracture Zone; a less developed zone of thin crust is observed on the conjugate flank of the MAR just east of the Lesser Antilles island arc. Farther south, a prominent ~400 km wide zone of generally thin crust is centered along the Chain Fracture Zone. Elsewhere, scattered small areas of thin crust are associated with major fracture zones. Notably, modeled crust is also thin along the MAR ridge axis south of 30°N and south of the Charlie Gibbs Fracture Zone. As discussed later, at least part of this is likely an artifact of our thermal model. Overall, thin crust is observed over 7% of the total area of ocean crust in the North Atlantic and it accounts for 4% of the total crustal volume in this area (Table 3).

4.2. Normal Crust

[28] Normal crust (Figure 7), here defined as crust 4–7 km thick, constitutes 58% of the total crustal area and 47% of the total crustal volume in the North Atlantic between the Chain Fracture Zone and 76°N (Table 3).

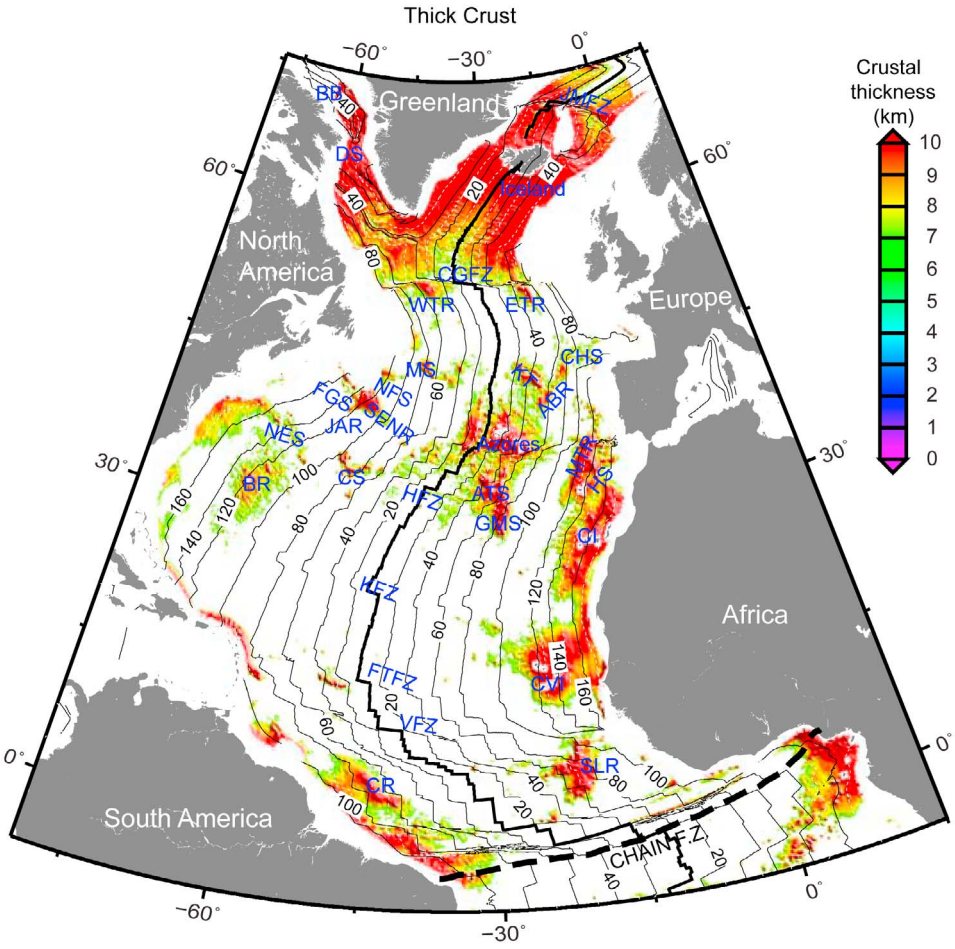

Figure 8. Map of modeled crustal thickness for areas of thick crust (>7 km).

4.3. Thick Crust

[29] Based on our crustal thickness model, about 35% by area of the North Atlantic Ocean crust is identified as thickened (>7 km) (Figure 8), and it accounts for 49% of the total volume of ocean crust in the North Atlantic (Table 3). Of this 49%, by far the largest proportion (44% of the total crustal volume) is associated with well-known melt anomalies. The remaining 5% is in regions that do not have clear correlations with known hot spots. We integrated areas and volumes for individual regions; results are shown in Figure 11 and Table 4.

5. Discussion

5.1. Thin Crust in the North Atlantic

[30] As previous studies [e.g., *Reid and Jackson*, 1981; *Bown and White*, 1994] have shown, there is a correlation between reduced crustal thickness and very slow spreading rates, and this might help to explain the main zones of thin crust between 20°N and 28°N on the two flanks of the MAR (Figure 6). Although there is some variation, the overall spreading half rate between 80 and 40 Ma was relatively low (~16 mm yr^{-1}; Figure 1b) [*Müller et al.*, 2008], while at 110 to 80 Ma it was nominally ~24 mm yr^{-1}. The latter rate is an average for the Cretaceous magnetic quiet period (~125 to 80 Ma), which lacks internal chrons that would allow determination of true, shorter-term rates. Thus, it is possible that the rate in the younger part of the quiet zone was lower than 24 mm yr^{-1} and that low rates overall contributed to formation of relatively thin crust between ~110 and 40 Ma. This explanation, however, is unsatisfactory. First, the crust is too thin for even a rate of ~16 mm yr^{-1} in ~80–40 Ma crust. *Bown and White* [1994] suggested that crustal thickness is relatively normal except for very slow rates of <7.5 mm yr^{-1} and therefore the crust

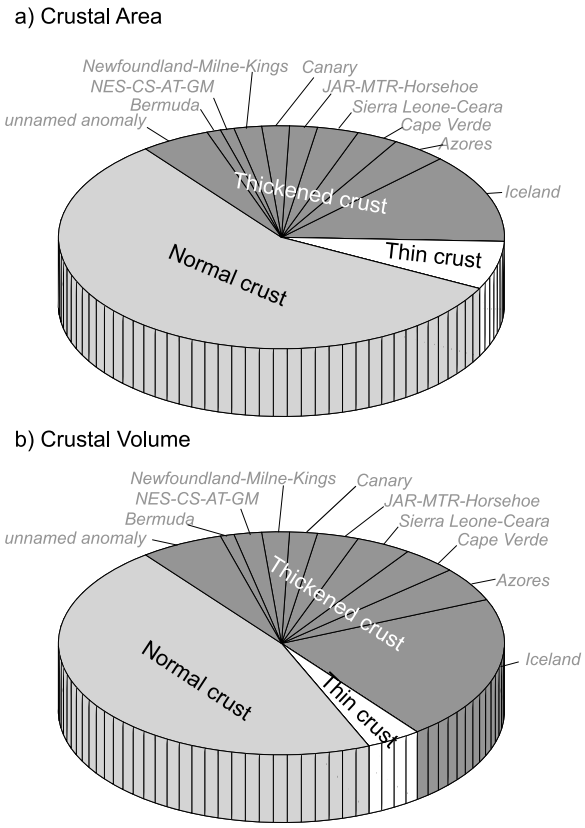

Figure 9. (a) Area and (b) volume of North Atlantic crust, with area of thickened crust subdivided according to seafloor provinces.

between 80 and 40 Ma should not be obviously thinner than in other areas. Second, modeled crust of normal thickness is present between 40 Ma and 0 Ma at the same latitude (~20°N–28°N), but the spreading half rate during this period was even lower (~13 mm yr^{-1} on average) than that between 80 and 40 Ma. Thus, spreading rate dependence of crustal thickness appears not to explain the observed zones of thin crust.

[31] *Ruedas and Schmeling* [2008] modeled the interaction of accretion and strain at spreading axes and concluded that thin crust is produced when the accretion zone is narrower than the strain zone. This is the common configuration along the MAR outside areas influenced by the Iceland and Azores hot spots. Thus we expect to see this effect broadly manifested in the North Atlantic. However, the zone of thin crust at 20°–28°N is latitudinally restricted, which suggests that the zone was not produced by this mechanism.

[32] Another possibility is that the zone of thin crust was a result of reduced magma supply from relatively cold or refractory mantle at the MAR axis as shown in Figure 12a. This should produce symmetrical zones of thin crust on the conjugate ridge flanks, which we do observe in broad scale, although not in detail. It is well established that lateral changes in mantle temperature, water content, and composition occur at scales up to hundreds of kilometers in the North Atlantic [e.g., *Schilling*, 1985; *Bonath*, 1990; *Bonatti et al.*, 1992], so this mechanism is reasonable.

[33] An additional, related consideration is that the apparently thin crust may be at least in part an artifact resulting from our modeling assumptions. We assumed a constant mantle density of 3.3×10^3 kg m^{-3} throughout the North Atlantic, but somewhat higher actual mantle density in this region, related for example to the presence of cold mantle, would produce our modeled result of thinner crust and it would also explain the associated depth anomaly (Figure 3b). Observed departures from cross-axis symmetry might be explained by differences in cooling history of the mantle on the two sides of the MAR, possibly as a result of differing patterns of faulting and off-axis hydrothermal circulation. All these arguments may apply equally well to the conjugate zones of thin crust between the Fifteen Twenty and Vema fracture zones (Figure 6).

[34] The broad zone of apparently thin crust centered around the Chain Fracture Zone probably can be attributed to similar causes. *Bonatti et al.* [1993]

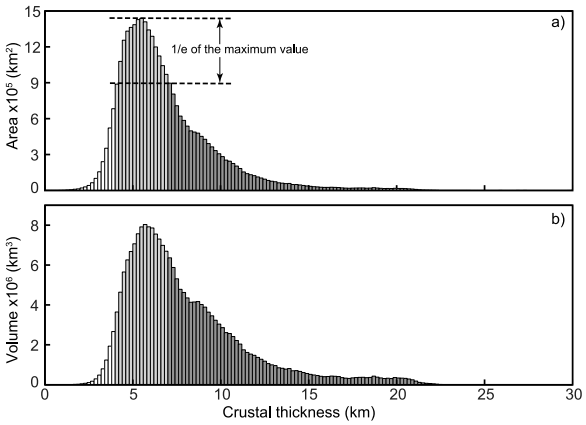

Figure 10. Distribution of (a) integrated ocean crustal area and (b) volume in the North Atlantic as a function of crustal thickness at 0.2 km intervals. Peak value in the crustal thickness distribution is 5.5 km for the North Atlantic. Crustal thickness values of 4.12 and 7.04 km, respectively, correspond to (1–1/e) of the peak value. We use rounded values of 4 km and 7 km as boundary values between thin, normal, and thick crust. Shading: thin crust (<4 km, white bars), normal crust (4–7 km, gray bars), and thickened crust (>7 km, dark bars).

Table 3. Crustal Thickness Distribution

	Crustal Thickness			
	Thin[a] (<4 km)	Normal (4–7 km)	Thick (>7 km) Associated With Hot Spots	Thick (>7 km) Unassigned
Crustal Area (km^2)	2.24×10^6	1.84×10^7	9.79×10^6	1.25×10^6
Crustal Area/Total Area[b]	7%	58%	31%	4%
Crustal Volume (km^3)	7.84×10^6	1.01×10^8	9.52×10^7	1.13×10^7
Crustal Volume/Total Volume[c]	4%	47%	44%	5%

[a]About one fourth of the thin crust lies along the MAR axis, and some of this thin crust might be an artifact of our thermal model, which ignored near-ridge-axis hydrothermal cooling.
[b]Total area of oceanic crust is 3.17×10^7 km^2.
[c]Total volume of oceanic crust is 2.16×10^8 km^3.

documented cold, undepleted mantle and a low degree of mantle melting in this region. The reduced melt supply would result in accretion of thin crust (Figure 12a), while the increased density of the cold mantle would enhance "crustal thinning" in our model results as noted above.

[35] In contrast to the above areas, the presence of thin crust off the Nova Scotia margin is substantiated by seismic results (see Figure S3, profiles 15 and 16) and however, it is not matched by any kind of thin crust in its conjugate off Morocco (Figure 6). It is likely that both the Moroccan crust and its Nova Scotian conjugate were originally accreted at the MAR axis above relatively cold or refractory mantle but the Moroccan margin could later be strongly affected by off-axis melt anomalies.

[36] Finally, we consider the apparently thin crust along the MAR axis south of about 30°N and south of the Charlie Gibbs Fracture Zone (Figure 6). Comparison of our modeled crustal thickness with on-axis seismic results south of Kane Fracture Zone (Figure S3, profiles 5 and 6) shows that the modeled thickness is consistently less than the seismic thickness. At least some of the thin model crust may be an artifact of our thermal model at the ridge axis, which does not take into account hydrothermal cooling there; it thus commonly overpredicts negative MBA values, resulting in under prediction of crustal thickness (see, for example, profiles 14, 15, and 17 in Figure S2).

5.2. Thickened Crust Associated With Melt Anomalies

[37] We divide areas of thickened crust into three categories, as follows.

[38] The first category is thickened crust symmetrical about the MAR axis. Symmetrical crustal thickening on the flanks of the ridge is attributed to enhanced melt supply at the ridge axis. Prominent examples include pronounced thick crust created by interaction between the (on-axis) Iceland hot spot and the (off-axis) Azores hot spot and Mid-Atlantic Ridge (Figure 12c); and thick crust at the conjugate West and East Thulean rises, Sierra Leone and Ceara rises, and J Anomaly Ridge and Madeira-Tore Rise.

[39] The second category is thickened crust along hot spot tracks. As a plate moves relative to an underlying plume, a volcanic trail can be produced on the plate; this trail is not symmetrical about the MAR axis provided that the hot spot is not located at the axis (Figure 12c). A typical example in our study area is the New England–Corner–Atlantis–Great Meteor Seamount chain (Figure 8). Volcanic

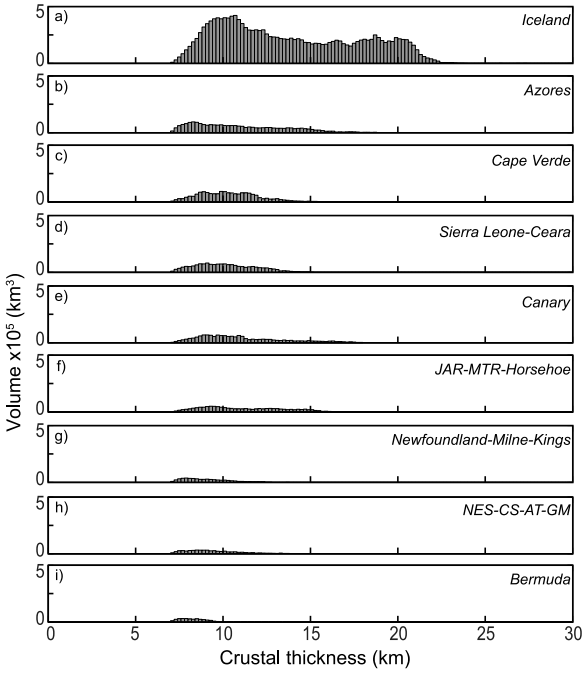

Figure 11. Bar plots showing distribution of excess crustal thickness (in excess of 7 km thick, 0.2 km intervals) for individual areas affected by melt anomalies.

Table 4. Crustal Volumes and Areas for Individual Regions of Thickened Crust

Region	Regional Total Area (km^2)	Regional Total Area/North Atlantic Total Area[a]	Regional Total Volume[b] (km^3)	Regional Total Volume/North Atlantic Total Volume	Regional Excess Volume[c] (km^3)	Regional Excess Volume/North Atlantic Excess Volume[d]
Iceland	4.11×10^6	13%	4.53×10^7	21%	1.65×10^7	57%
Azores	1.30×10^6	4%	1.15×10^7	5%	2.36×10^6	8%
Cape Verde	9.00×10^5	3%	8.19×10^6	4%	1.89×10^6	6%
Sierra Leone–Ceara	9.42×10^5	3%	8.28×10^6	4%	1.68×10^6	6%
Canary	6.64×10^5	2%	6.24×10^6	3%	1.59×10^6	5%
J Anomaly Madeira Tore–Horseshoe	4.99×10^5	2%	4.70×10^6	2%	1.21×10^6	4%
Newfoundland–Milne–Kings Trough	4.94×10^5	2%	3.9×10^6	2%	5.13×10^5	2%
New England–Corner–Atlantis–Great Meteor	4.53×10^5	1%	3.72×10^6	2%	5.49×10^5	2%
Bermuda	4.23×10^5	1%	3.27×10^6	1%	3.12×10^5	1%
Unassigned Crustal Thickness Anomalies	1.25×10^6	4%	1.13×10^7	5%	2.62×10^6	9%

[a]Regional total area is the area with crustal thickness > 7 km.
[b]Area of the region × crustal thickness of the region.
[c]Area of the region × crustal thickness in excess of 7 km.
[d]Atlantic excess volume is the Atlantic area with crust >7 km thick × crustal thickness in excess of 7 km.

features produced by the Canary and Madeira hot spots also show an asymmetrical pattern.

[40] The third category is isolated anomalies with no clear hot spot association: These are anomalies that do not show clear evidence for either a volcanic track or interaction with the MAR axis. The thickened crust found at Bermuda and possibly at the Cape Verde Islands lack apparent hot spot tracks and seems to be related to isolated melt anomalies.

5.2.1. Symmetrical Off-Axis Features Generated by MAR-Centered Melt Anomalies

5.2.1.1. West and East Thulean Rises

[41] The West and East Thulean rises are located just south of the Charlie Gibbs Fracture Zone and were formed at the MAR axis between 58 and 53 Ma [*Vogt and Jung*, 2005]. Crustal thickness south of the fracture zone is less than 7 km except at these two rises. Thickened crust at the rises appears abruptly at ~55 Ma and trends parallel to the seafloor isochrons. The crust thins gradually in younger seafloor, with thickened crust persisting the longest near the fracture zone. Overall, the area of thickened crust at the East Thulean Rise is less than that of the West Thulean Rise.

[42] *Vogt and Jung* [2005] proposed that this ridge pair was formed over a mantle source of high fertility. An alternate possibility is that melt from the Iceland hot spot reached across the fracture zone to form the rises, despite a transform offset of ~270 km at the time [*Klitgord and Schouten*, 1986]. There is some support for this idea in that crust associated with the Iceland hot spot north of the fracture zone is thickest between about 60 and 40 Ma and has thinned progressively since that time (Figure 8). In either case, the pattern of crustal thickness at the rises suggests that the onset of melt input was abrupt and that it tapered off over a period of ca. 15 Myr.

5.2.1.2. Sierra Leone–Ceara Rises

[43] The conjugate Sierra Leone and Ceara rises lie at ages of >80 Ma to ~60 Ma and have crust 8–15 km thick. The Ceara Rise forms an elongated band of thick crust that extends more than 700 km from northwest to southeast with a width of ~200–300 km (Figure 8). The conjugate Sierra Leone Rise is somewhat broader and irregular in shape, but it exhibits an overall NE-SW trend. The length and width of the Sierra Leone Rise are roughly similar to those of the Ceara Rise.

[44] These two rises are thought to have formed at the MAR axis, probably because of excessive magmatism related to the presence of fertile mantle [*Vogt and Jung*, 2005]. *Schilling et al.* [1994] attributed a La/Sm anomaly along the MAR axis, now centered at 1.7°N ± 300 km, to a "Sierra Leone plume" that constructed the Ceara and Sierra Leone rises by plume-ridge interaction between 75 and 48 Ma. The southward and ridgeward trends of the two rises, as well as similar, continuing trends

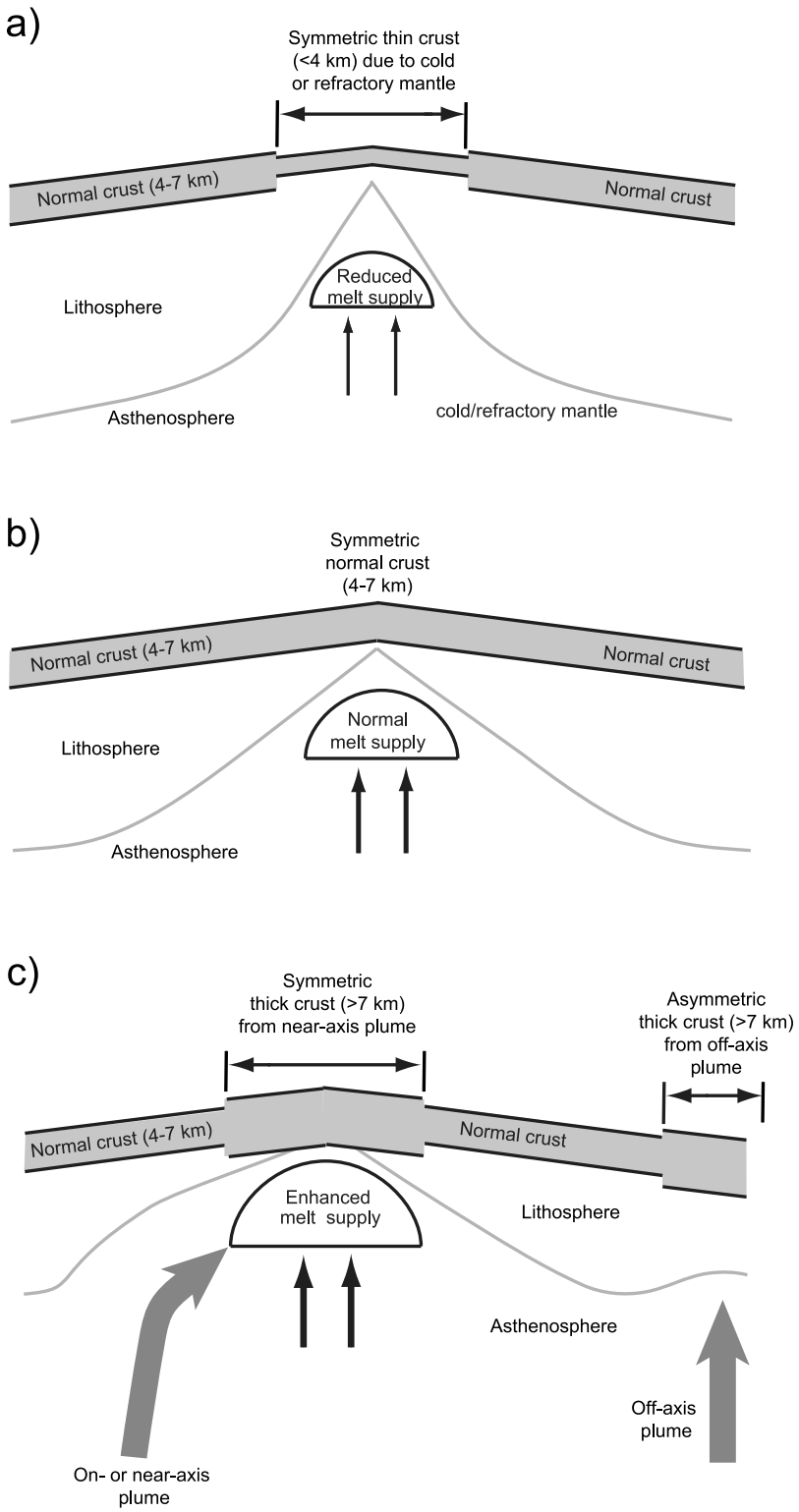

Figure 12. (a) Schematic diagram showing that thin crust is emplaced at the ridge axis above relatively cold or refractory mantle. (b) Schematic diagram of normal crust accretion at the ridge axis. (c) Schematic diagram showing that thick crust is produced when affected by melt anomaly (e.g., plume).

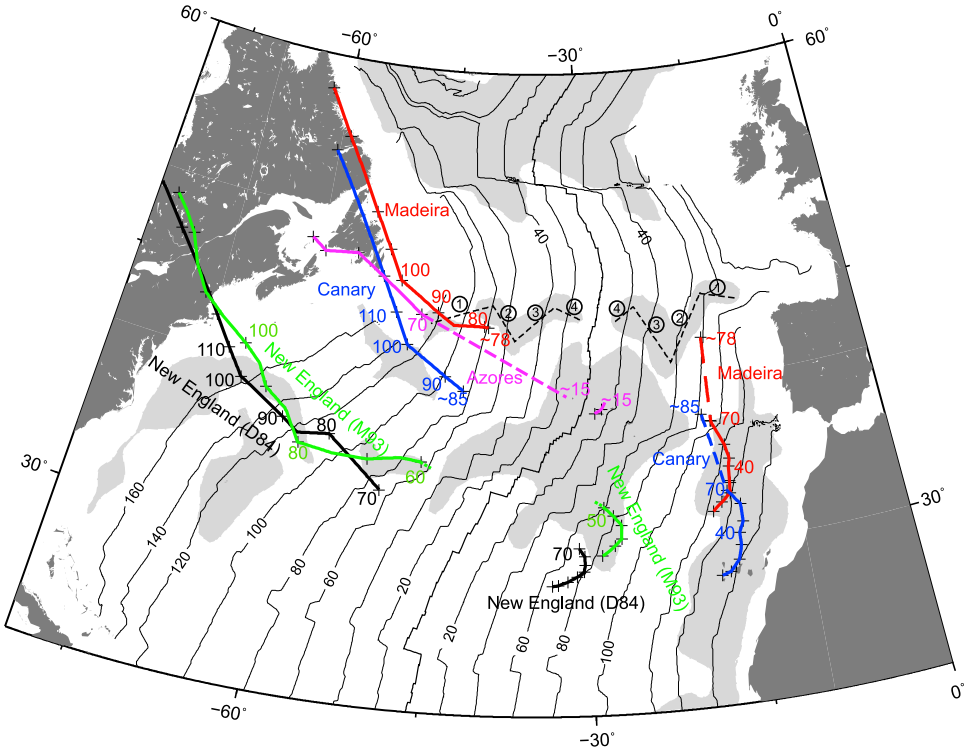

Figure 13. Major hot spot tracks in the North Atlantic. Red, blue, purple, and black solid lines are tracks for Madeira, Canary, Azores, and New England hot spots, respectively, based on the model of *Duncan* [1984]. Dashed lines are revisions made to *Duncan*'s [1984] model in order to show where age intersections of the hot spot tracks with corresponding crustal isochrons would result in transfer of the hot spot track from the North American to the Eurasian and African plates. Green solid line follows the track of New England hot spot calculated by *Müller et al.* [1993]. New England (D84) and New England (M93) refer to the New England hot spot track of *Duncan* [1984] and *Müller et al.* [1993], respectively. Ages along tracks are shown by crosses at 10 Myr intervals. Black dashed lines with circled numbers denote the "M shape" traces of a band of thick crust associated with the Newfoundland-Milne seamounts, Kings Trough, and the Azores-Biscay Rise. Gray-shaded areas show areas of thick crust (>7 km) from Figure 8, with smoothed boundaries.

of scattered patches of thick crust at younger ages (Figure 8), suggest a southward propagation of the magma source relative to the MAR axis that is consistent with the "Sierra Leone plume" hypothesis.

5.2.1.3. J Anomaly Ridge and Madeira-Tore Rise

[45] The J Anomaly Ridge (JAR) and Madeira-Tore Rise (MTR) are conjugate features that are located on old (~130–120 Ma) oceanic crust and extend parallel to isochrons. The northern end of the J Anomaly Ridge merges with the NW-SE trending Southeast Newfoundland Ridge (Figure 8). The Fogo seamounts are minor features associated with thickened crust to the west. This group of features forms a pseudotriangular zone of thick crust with a thin tail extending northwestward along the southwest margin of the Grand Banks. In the eastern Atlantic, the Madeira-Tore Rise is part of a region of thickened crust that includes the Horseshoe Seamount chain. This area extends northward to ~40°N and southward to ~32°N between the 120 and 150 Ma isochrons.

[46] *Tucholke and Ludwig* [1982] interpreted the JAR and MTR as paired aseismic ridges formed at the MAR axis when it encountered a large magma source (possibly a mantle plume) beneath the southern edge of the Grand Banks–Iberia rift system. This magmatism also formed thick crust at the Southeast Newfoundland Ridge [*Tucholke and Sibuet*, 2007]. The conjugate JAR and MTR are suggested to have formed above the Canary hot spot [*Geldmacher et al.*, 2006]. However, the Canary hot spot did not pass the JAR until about 100 Ma according to *Duncan* [1984] (Figure 13), which is more than 20 Myr later than the formation of the JAR (prior to late Barremian–early Aptian, ca. 121–125 Ma [*Tucholke et al.*, 1979; *Tucholke and Ludwig*, 1982]).This implies that the Canary hot spot was not the magma source for the conjugate ridges. To the west, an $^{40}Ar/^{39}Ar$ age of 130.3 ±

1.3 Ma was determined for a basalt clast dredged on the flanks of one of the Fogo seamounts along the southern margin of the Grand Banks [*Pe-Piper et al.*, 2006]. This age is closer to, but still older than, the proposed timing for the passage of the Canary hot spot. As an alternate to hot spot volcanism, *Pe-Piper et al.* [2007] suggested that the Fogo seamounts were formed by magmatism associated with margin tectonics, specifically small-scale mantle upwelling related to an edge effect of the transform transition between the spreading ocean and the continental block. Based on available evidence, it seems likely that the JAR-MTR conjugates were formed above an ephemeral melt anomaly at the MAR axis, perhaps later enhanced by passage of the Canary hot spot.

5.2.2. Symmetrical Features: The Present On- and Near-Axis Hot Spots

5.2.2.1. Iceland

[47] Among the hot spot–influenced regions, the most prominent is associated with the Iceland hot spot that occupies a huge area north of the Charlie Gibbs Fracture Zone (CGFZ) (Figure 8). Thick crust (generally 10–15 km, locally > 20 km) has been generated on both flanks of the Reykjanes and Kolbeinsey Ridges since ~50 Ma, with a maximum thickness exceeding 25 km where the hot spot is now located east of central Iceland [*Lawver and Müller*, 1994]. In general, these values are in agreement with seismic studies (e.g., 11 km at ~63°N in Reykjanes Ridge and 21 km in southwest Iceland [*Weir et al.*, 2001]; ~9 km on 1–2 Ma old flank of Kolbeinsey Ridge [*Kodaira et al.*, 1997]). Crustal thickness at the MAR axis decreases northward from Iceland to the Jan Mayen Fracture Zone (JMFZ) with a gradient of ~0.02 km/km. Southward thinning of ~0.012 km/km is observed from Iceland to the CGFZ. The influence of the Iceland hot spot on the rest of the North Atlantic Ocean basin seems to have been blocked by the Charlie Gibbs Fracture Zone, with the possible exception of the West and East Thulean rises as previously discussed. At the northern end of the Iceland hot spot influence, the JMFZ may have acted as a "leaky barrier" to along-axis melt transport to the north. Large portions of the seafloor older than ~20 Ma north of the JMFZ have thickened crust and seem to have been influenced by the hot spot, although there is a clear decrease in crustal thickness across the fracture zone. There has been a significant decrease in crustal thickness north of the fracture zone since ~20 Ma, roughly synchronous with the decrease south of Iceland near the CGFZ. Seismic refraction study has shown that the oceanic crust for ages between 0 and 22 Ma off the ultraslow spreading Mohns Ridge has a thickness of 4.0 ± 0.5 km [*Klingelhöfer et al.*, 2000]. We infer these observations might imply that there has been a waning of melt supply from the Iceland plume over the past ~20 Myr.

[48] The influence of the Iceland hot spot was not confined to the MAR, but is also evident in the Labrador Sea, Davis Strait, and Baffin Bay. Thicker than normal crust is modeled throughout these areas. The first effects of the hot spot appeared between Greenland and Baffin Island about the time that the Labrador Sea and Baffin Bay began to open. Large volumes of basaltic lavas are present in eastern Baffin Island and along the west Greenland coast in the area of Disko Island [*Clarke*, 1970], and dates on interbedded sediments suggest that the oldest volcanic rocks have an age of 64.4 Ma [*Larsen et al.*, 1992]. In east Greenland, the first extrusion of flood basalts occurred between 57 and 53 Ma [*Noble et al.*, 1988]. *Larsen et al.* [1999] proposed that the near simultaneous onset of volcanism at the west and east Greenland margins can be explained by fast horizontal spreading of the plume head when it impinged on the lithosphere, with the location of the stem remaining stationary under Greenland. *White and McKenzie* [1989] proposed that the plume was located under east Greenland and that volcanism in the adjacent continental areas is explained by lithospheric stretching and thinning above a thermal anomaly in the mantle. *Lawver and Müller* [1994] computed the hot spot path of Iceland since 130 Ma by keeping it fixed relative to major hot spots beneath the African, Indian-Australian, and North American plates. Their results suggest that the Iceland hot spot was located beneath the western margin of Greenland between 70 Ma and 60 Ma and beneath the eastern margin at 40 Ma, but this track does not fit the observed ages of volcanism very well. *Norton* [2000] proposed that the Iceland hot spot is in fact not fixed to the other Indo-Atlantic hot spots, which could allow for a track that better fits the volcanic ages. Whichever may be the case, the crustal thickening effects of the Iceland hot spot have extended far beyond the immediate vicinity of any likely track. From the northern part of Baffin Bay to the southern end of the Labrador Sea, and from west to east Greenland, the hot spot influence has extended more than 1,000 km both latitudinally and longitudinally.

5.2.2.2. Azores

[49] The second most important crustal thickness anomaly is associated with the Azores hot spot (Figure 8). The area affected by the Azores hot spot extends northward to the Milne seamounts–Kings Trough–Azores-Biscay Rise chain and southward to about 30°N. Rayleigh wave dispersion analysis by *Searle* [1976] showed that the crust of the Azores Plateau is about 60% thicker than "normal" oceanic crust and we find from our gravity analysis that crust >15 km thick is present in the shallowest parts of the plateau. The rift valley of the MAR on the Azores Plateau is observable on Figure 8, separating the plateau into two parts. The influence of the hot spot along the MAR axis extending southward is characterized by a decrease in crustal thickness of ~0.015 km/km. The northward gradient is steeper, with a value of ~0.03 km/km.

[50] Crustal thickening in the Azores region began at about 50 Ma to the south of the Azores triple junction on the North American plate but occurred progressively later toward the north, where it is observed at about 25–20 Ma. These observations are consistent with findings of *Gente et al.* [2003] that plateau formation began about 20 Ma in the northern area.

[51] The older thickening toward the south is part of a trend extending from the Corner seamounts into the southwest Azores Plateau and is probably associated with the New England hot spot, as discussed later in section 5.2.3.4. Thickening on the African plate south of the Azores is observed in crust as old as 90 Ma; this is associated with the prominent Atlantis–Great Meteor Seamount groups, which are also a product of the New England hot spot. The main Azores Plateau east of the MAR axis encompasses the triple junction between the North American, Eurasian-Iberian and African plates. Crustal thickness patterns in this area have been complicated by intense tectonic activity which has resulted in thickened crust, mainly concentrated at the plate boundary [*Rovere et al.*, 2004]. This thick crust extends out to ~80 Ma on the northeastern flank of the plateau.

[52] The widespread, thick crust area centered on the Azores Plateau has been attributed to the interaction between the Azores hot spot and seafloor spreading at the MAR axis [*Cannat et al.*, 1999; *Gente et al.*, 2003]. The Azores hot spot is considered to be now located about 200 km east of the MAR axis, under the Azores archipelago [*Ito and Lin*, 1995]. Clearly observed low-velocity anomalies in the mantle, centered to the east of the MAR [*Zhang and Tanimoto*, 1992], suggest a similar location. Based on *Duncan*'s [1984] hot spot track, the Azores hot spot was once located in the Gulf of St. Lawrence (Figure 13). As the plates moved, the hot spot was overridden by the MAR axis at ~15 Ma [*Duncan*, 1984] and has remained close to the spreading ridge since then. However, we see no indication of thick crust that could be associated with a hot spot track to the west of the Azores Plateau. This suggests either that the activity of the hot spot was very intermittent or that the hot spot only developed within the past 20–30 Myr. *Silveira et al.* [2006] proposed that the plume beneath Azores is currently dying. This decrease in melt supply is consistent with our observation that the hot spot influence appears to have retreated along axis from south of the Hayes Fracture Zone well to the north in the last ~20 Myr (Figure 8).

5.2.3. Asymmetrical Hot Spot Effects

5.2.3.1. Newfoundland-Milne Seamounts, Kings Trough, and Azores-Biscay Rise

[53] Between 42°N and 45°N, a band of thickened crust with a N-S width of ~100–200 km extends from near the Newfoundland margin to the Bay of Biscay (Figures 8 and 13). From west to east on the west side of the ridge axis, the band includes the Newfoundland seamounts, the Milne seamounts, and a basement high oriented NE-SW and then slightly NW-SE. On the east side of the MAR axis, it extends northeast to the NW-SE trace of Kings Trough and then the SW-NE-oriented Azores-Biscay Rise before reaching eastward along the Charcot seamounts into the outer limits of the Bay of Biscay. Overall, the band follows a wide "M" shape on each side of the MAR axis, and this is symmetrical about the axis.

[54] It is tempting to attribute this symmetrical pattern to ridge-centered magmatism above a plume that migrated northward and southward along the axis. However, the pattern seems not to be related so simply to axial melt anomalies on the MAR.

[55] The first pair of legs consists of the Newfoundland seamounts and the northwestern part of the Milne seamounts on the North American plate and the Charcot seamounts on the Eurasian plate (Figures 8 and 13). The Newfoundland seamounts lie on crust ~130–110 Ma old that passed over the Madeira hot spot at about 95–85 Ma and over the Azores hot spot at ~70 Ma (Figure 13) [*Duncan*, 1984]. Considering the apparent age of the New-

foundland seamounts (one date of ~98 Ma [*Sullivan and Keen*, 1977]), they probably formed above the Madeira hot spot. This hot spot and the Azores hot spot did not cross the MAR axis until ~78 Ma and ~15 Ma, respectively (Figure 13). Then they moved south relative to the Eurasian-African plate, so they could not have formed the Charcot seamounts on >80 Ma crust. Instead, the Charcot seamounts are thought to have formed by volcanism associated with a triple junction that connected the MAR with a spreading center (now extinct) in the Bay of Biscay [*Williams*, 1975].

[56] The second pair of legs is formed by the southeast extension of the Milne seamounts and the conjugate Azores-Biscay Rise (Figures 8 and 13). These legs are positioned symmetrically about the MAR axis in a south directed V shape. One hypothesis for their origin is that they were generated on the MAR between ~76–56 Ma as a result of a ridge-centered, southward migrating melt anomaly [*Whitmarsh et al.*, 1982]. *Louden et al.* [2004] recognized the Milne seamounts and Azores-Biscay Rise from basement highs and attributed them to a Milne hot spot that was active from about 76 Ma to 53–36 Ma. According to *Duncan*'s [1984] hot spot model (Figure 13), the Madeira hot spot was close to the MAR axis and not far from the latitude of the Milne seamounts and Azores-Biscay Rise pair at ~80 Ma. Thus it is possible that the Madeira hot spot was the magma source for the formation of these conjugate crustal thickness anomalies.

[57] West of the Azores-Biscay Rise, Kings Trough forms a prominent feature oriented in a northwest-southeast direction, and its conjugate on the North American plate is a basement high [*Louden et al.*, 2004] with a mirror image trend. The resulting north pointing V-shaped feature (Figures 8 and 13) comprises the third pair of legs. Kings Trough was once the plate boundary between Eurasia and Iberia [*Srivastava et al.*, 1990] and is suggested to have formed as a shear zone by the northward propagation of the spreading rift, with the conjugate high on the western flank being the trace of the mirrored pseudofault [*Srivastava and Roest*, 1992]. As such, these legs have no apparent relation to a hot spot, although the thickened crust could have been associated with elevated melt production in fertile mantle rising at the plate boundary.

[58] Two southward trending bands of somewhat thinner crust that close to the present ridge axis constitute the fourth pair of legs (Figures 8 and 13). They are at the northern limit of thickened crust associated with the Azores hot spot. They might have originated from a fertile mantle source that migrated south along the MAR axis. Alternately, the pattern could have been generated by decreasing influence of the Azores hot spot with time; this would be consistent with the similar decrease observed along the southern margin of the Azores Plateau.

[59] In summary, although the features discussed above exhibit a remarkably symmetrical pattern about the MAR axis, they have resulted from a mixture of volcanism and tectonic effects. The Madeira and possibly the Azores hot spot appear to have contributed to parts of the pattern at different times.

5.2.3.2. The Madeira Hot Spot

[60] The Madeira hot spot passed from the northeast coast of Canada beneath the Grand Banks and Newfoundland Basin and was located under the North American plate until ~78 Ma (Figure 13) [*Duncan*, 1984]. Based on our observations (Figure 8), the Newfoundland seamounts and perhaps the Milne seamounts are the only features associated with the Madeira hot spot on the North American plate. The gap between Newfoundland and the Milne seamounts suggests episodic activity of the hot spot. After it was crossed by the MAR at ~78 Ma, the relative motion of the hot spot was southward beneath the Eurasian and then the African plate, passing by the southern part of the Madeira-Tore Rise and terminating at the southern end of the Horseshoe seamounts (Figure 13) [*Duncan*, 1984]. The NNE-SSW oriented Horseshoe seamounts have ages of ~67 to 5 Ma, progressively decreasing from north to south [*Geldmacher and Hoernle*, 2000], which is consistent with the time and motion of the Madeira hot spot.

5.2.3.3. The Canary Hot Spot

[61] South of the Madeira province, the Canary hot spot produced a track (Canary Islands) with orientation and age progression (~68–3 Ma) similar to that of the Madeira hot spot [*Geldmacher et al.*, 2001] after it crossed the MAR axis at ~85 Ma (Figure 13) [*Duncan*, 1984]. Late Cretaceous volcanic rocks (~80–95 Ma) from the Madeira-Tore Rise show isotopic compositions similar to those from the Canary Islands [*Geldmacher et al.*, 2006], providing evidence that the Canary hot spot passed through the Madeira-Tore Rise during that time and generated overprinting volcanism. In contrast to its readily identified hot spot track on the African plate, no clear indicator of a volcanic track associated with the Canary hot spot is found on the North American plate. According to Duncan's calculated track (Figure 13) [*Duncan*, 1984], the Canary hot

spot passed near the Fogo seamounts and the J Anomaly Ridge between ~120–100 Ma. However, as already discussed (section 5.2.1.3), this does not fit the ages of the Fogo seamounts (~130 Ma [*Pe-Piper et al.*, 2006]) and the J Anomaly Ridge (older than 118 Ma [*Tucholke and Ludwig*, 1982]). Thus the volcanism on the African plate seems to be the only surface expression of the Canary hot spot, suggesting that the hot spot might not have been active until it was overridden by the African plate.

[62] Both the Madeira and Canary hot spots produced significantly thickened crust on the eastern side of the MAR. This can mainly be attributed to the slow absolute motion of the African plate over the hot spots [*Müller et al.*, 1993].

5.2.3.4. New England, Corner, Atlantis, Cruiser, and Great Meteor Seamounts

[63] The New England seamounts are associated with a narrow belt of ~8–10 km thick crust that starts near the U.S. east coast margin and extends ESE to near the 100 Ma isochron (Figure 8). There is a ~300 km gap between the New England seamounts and Corner seamounts, which lie between 53°W and 47°W and are associated with thickened crust that generally parallels the Hayes Fracture Zone. In the eastern Atlantic a group of seamounts positioned north and south of the Hayes Fracture Zone, including the Atlantis, Cruiser, and Great Meteor seamounts, are genetically related to the New England seamounts and Corner seamounts [e.g., *Tucholke and Smoot*, 1990], and these seamounts are associated with a band of thickened crust that trends slightly NNW-SSE. This band is coincident with the southeast part of the area influenced by the Azores hot spot and has a crustal thickness >10 km, thicker than that associated with the seamounts in the western North Atlantic.

[64] The New England seamounts form a northwest-southeast trending volcanic track with decreasing age (~103–82 Ma) toward the southeast [*Duncan*, 1984] (Figure 13), reflecting northwest motion of the North American plate over the New England hot spot between about 110 and 80 Ma. The Corner seamounts farther to the east also lie on the track of the New England hot spot at ca. 80 Ma [*Duncan*, 1984; *Müller et al.*, 1993] (Figure 13). Seamount subsidence analysis estimated a formation age of the Corner seamounts at ~80–76 Ma [*Tucholke and Smoot*, 1990], which is consistent with this correlation. As the central Atlantic opened, the New England hot spot was crossed by the MAR at ~70–60 Ma and it then generated an arcuate track to the south on the African plate, forming the Atlantis and Cruiser seamounts, and ending at the Great Meteor Seamount [*Duncan*, 1984].

[65] Two important features are worth noting. First, volcanism above the hot spot seems to have been episodic, much like the episodic behavior of the Madeira hot spot suggested by the gap between the Newfoundland and Milne seamounts. For example, the Corner seamounts are separated from the New England seamounts by ~300 km, and there is no indication of crustal thickening between them (Figure 8). Second, the hot spot track on the African plate is associated with much thicker crust than that on the North American plate. Although part of this is because of overlap with the area affected by the Azores hot spot, much of this thickening is probably due to the slow absolute motion of the African plate over the New England hot spot [e.g., *Müller et al.*, 1993], which for a given melt flux will result in increased crustal volume per unit area of seafloor.

5.2.4. Isolated Crustal Thickness Anomalies: Hot Spot or Non–Hot Spot Processes?

5.2.4.1. Bermuda

[66] The Bermuda Rise is associated with thickened crust over an area ~250 km wide that is elongated ~500 km along crustal isochrons (Figure 8). The uplift of the rise initiated at ~40–45 Ma [*Tucholke and Vogt*, 1979; *Jaroslow and Tucholke*, 1994] and was followed by volcanism that continued until about 25 Ma [*Vogt and Jung*, 2007]. The thickened crust associated with the Bermuda Rise seems to be isolated, with no obvious relation to nearby features and no indication of volcanism associated with a prior or later hot spot track. Furthermore, the elongation of thickened crust along crustal isochrons (Figure 8) conflicts with a fixed hot spot model that predicts a hot spot track orthogonal to the isochrons [e.g., *Vogt*, 1991]. *Detrick et al.* [1986] suggested that these observations could be explained by transient hot spot activity and relative motions between a Bermuda hot spot and the overlying North American plate. However, non–hot spot alternatives such as an "edge-driven" convection model [e.g., *Vogt*, 1991] seem to provide a better explanation for the isolation, location, and orientation of thickened crust at the Bermuda Rise.

5.2.4.2. Cape Verde

[67] The Cape Verde Rise lies ~500 km west of Africa and is the center of a prominent, pseudocir-

cular, thick crust region with a diameter of ~700 km (Figure 8). It is suggested to have been formed by a Cape Verde hot spot beginning around 22 Ma [*Holm et al.*, 2008]. It occupies a position near rotation poles of the slowly moving African plate over the hot spot reference frame [e.g., *Pollitz*, 1991; *Müller et al.*, 1993; *Kreemer*, 2009], implying that the Cape Verde hot spot is almost stationary with respect to the African plate. Thus the islands in this region do not form a linear chain with obvious age progression. Instead, melt input has produced a broad zone of thickened crust (Figure 8).

5.3. Correlation With Mantle Tomography

[68] Hot spots are surface manifestations of upwelling mantle plumes that might be detected by seismic tomography studies. For example, the Iceland hot spot has been shown to be located above a cylindrical zone of low-velocity anomalies in the upper mantle down to at least 400 km [*Wolfe et al.*, 1997]. Despite discrepancies in depth and extent of low-velocity anomalies between different tomographic models, there is a reasonably good regional correlation between the thickened crust that we associate with hot spots and the existence of low-velocity anomalies in the underlying mantle [e.g., *Zhao*, 2001; S. P. Grand, Data publicly available at global tomography, March 2010, www.geo.utexas.edu/faculty/grand/global_tomography.htm, 2003] that presumably are associated with hotter, more melt-rich mantle. The major exception is the Baffin Bay–Labrador Sea region, where hot spot volcanism took place mainly before 60 Ma. Changes in mantle structure due to convection over the long time interval since that event may explain why there is no associated low-velocity anomaly in the mantle. Comparison of observed thick crust regions with mantle tomography at finer scales is not possible because the tomographic models lack resolution at these scales.

5.4. Comparison With Isostatic Crustal Thickness North of 30°N

[69] Our study area overlaps with an area (30°–70°N, 0°–70°W) where isostatic crustal thickness calculations were made by *Louden et al.* [2004]. *Louden et al.* [2004] calculated anomalous basement topography (similar to our Figure 3b) after correcting for the effects of isostatic sediment loading and conductive plate cooling. They then calculated crustal thickness assuming isostatic compensation after removing dynamic topography from the anomalous basement depth. Overall, our results and those of *Louden et al.* [2004] show, qualitatively, consistent patterns in the spatial distribution of thickened crust. Our gravity-derived crustal thickness variations are smaller in amplitude than those determined from isostatic calculations by *Louden et al.* [2004], and there are differences in details of crustal thickness distribution patterns for specific regions (Figure 14). Also, our results give more reasonable crustal thickness values for margins (e.g., Nova Scotia, Morocco, and Iberia margins) where the isostatic calculations indicate zero to negative crustal thicknesses. These kinds of differences are not surprising, considering that our respective analyses differ in terms of sediment thickness data sets used, method of determining sediment unloading, and assumptions and parameters used to make crustal thickness calculations. Furthermore, the assumption of local isostasy might not work well for off-ridge-axis features that were accreted on lithosphere of considerable strength.

6. Conclusions

[70] Gravity-derived crustal thickness models were obtained from residual mantle Bouguer anomalies for the North Atlantic Ocean between 76°N and the Chain Fracture Zone. Normal crust, defined as 4–7 km thick, constitutes 58% of the total crustal area and 47% of the total crustal volume in North Atlantic. About 7% of the area (and ~4% of the volume) is identified as thin (<4 km) crust. Rough symmetry of thin crust zones about the MAR axis suggests that this crust was emplaced at the ridge axis above upwelling mantle that was relatively cold or refractory, which is consistent with geochemical observations of along-axis variations in melt supply at scales of hundreds of kilometers.

[71] Thickened crust (>7 km) constitutes about 35% of the total area and ~49% of the volume of North Atlantic crust, and it is interpreted to be affected by melt anomalies. The most prominent anomaly by far is the region influenced by the Iceland hot spot, which accounts for 57% of the total excess crustal volume in the North Atlantic. The crustal thickness anomaly associated with the Azores hot spot is the second most important with 8% of the total excess crustal volume of the North Atlantic, followed by the Cape Verde Rise which contributes 6% of the excess volume. Small but significant melt anomalies (2–5% of the excess volume) are associated with the Madeira, Canary, and New England hot spots, with mantle melting that produced the J Anomaly Ridge–Madeira-Tore

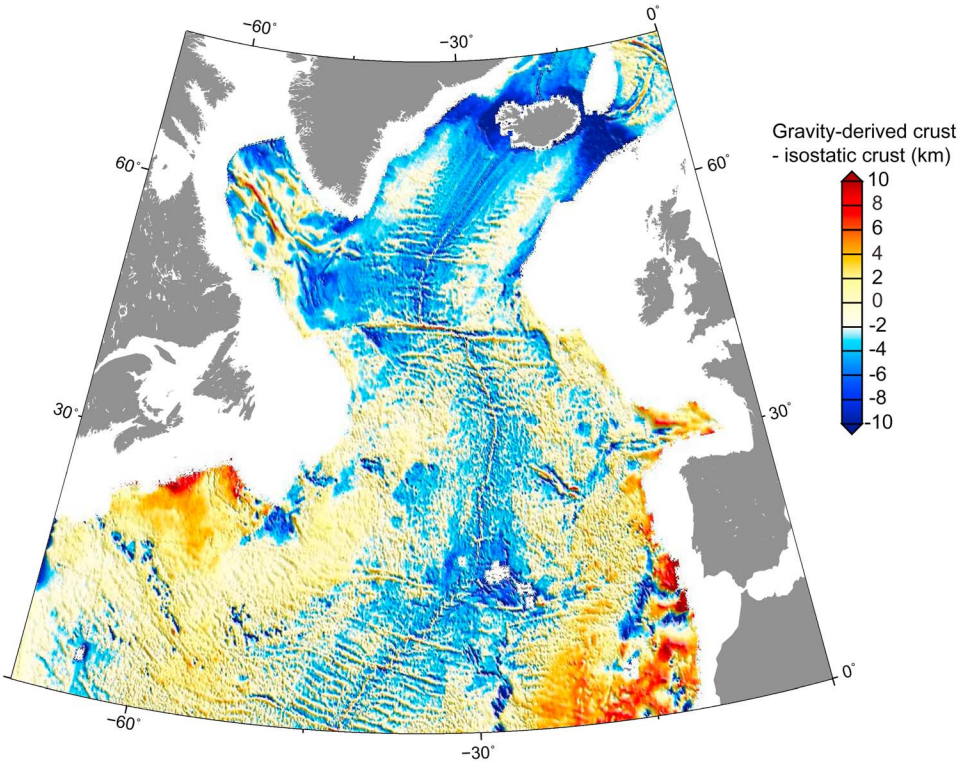

Figure 14. Difference map of our gravity-derived crustal thickness minus isostatic crustal thickness from *Louden et al.* [2004]. Our gravity-derived crustal thickness variations are smaller in amplitude than those determined from the isostatic calculations. In contrast to the isostatic calculations that gave negative crustal thickness for the margins [*Louden et al.*, 2004], our results give more reasonable values of crustal thickness for old oceanic crust near continental margins.

Rise, and with a likely hot spot that formed the conjugate Sierra Leone and Ceara rises. There are large crustal thickness variations along the tracks of these hot spots, indicating that their melt production was intermittent on time scales of tens of millions of years. Thickened crust exhibits both symmetrical and asymmetrical patterns about the MAR axis, which reflects whether melt anomalies were or were not centered on the MAR axis, respectively. The Bermuda and Cape Verde rises appear to be isolated features that have been produced by local melt anomalies with lifetimes of only ~20–25 Myr. Finally, crustal thickness anomalies observed on the African plate are larger than those on the North American plate, and we attribute this to the result of slower absolute plate speed of the African plate over relatively fixed hot spots.

Acknowledgments

[72] The bulk of this investigation was accomplished while Tingting Wang was a visiting student at the Woods Hole Oceanographic Institution, supported by a fellowship from the China Scholarship Council. We thank Daniel Lizarralde for providing locations of the SIGMA seismic lines, Tony Watts for suggesting the relationship between sediment thickness and depth, Dietmar Müller, Chuck DeMets, and Richard Gordon for supplying information on hot spot tracks in the North Atlantic, and Jian (Jasmine) Zhu and Tao Zhang for discussions. The GMT software of *Wessel and Smith* [1998] was used in producing figures. We appreciate review comments from Tim Minshull and two anonymous reviewers that greatly improved the paper. Additional support for this research was provided by the Charles D. Hollister Endowed Fund for Support of Innovative Research at WHOI (JL) and NSF China grants 40676023 and 40821062 (YJC).

References

Bonath, E. (1990), Not so hot "hot spots" in the oceanic mantle, *Science*, *250*, 107–111, doi:10.1126/science.250.4977.107.

Bonatti, E., A. Peyve, P. Kepezhinskas, N. Kurentsova, M. Seyler, S. Skolotnev, and G. Udintsev (1992), Upper mantle heterogeneity below the Mid-Atlantic Ridge, 0°–15°N, *J. Geophys. Res.*, *97*, 4461–4476, doi:10.1029/91JB02838.

Bonatti, E., M. Seyler, and N. Sushevskaya (1993), A cold suboceanic mantle belt at the Earth's equator, *Science*, *261*, 315–320, doi:10.1126/science.261.5119.315.

Bonatti, E., M. Ligi, D. Brunelli, A. Cipriani, P. Fabretti, V. Ferrante, L. Gasperini, and L. Ottolini (2003), Mantle thermal pulses below the Mid-Atlantic Ridge and temporal variations in the formation of oceanic lithosphere, *Nature*, *423*, 499–505, doi:10.1038/nature01594.

Bown, J. W., and R. S. White (1994), Variation with spreading rate of oceanic crustal thickness and geochemistry, *Earth Planet. Sci. Lett.*, *121*, 435–449, doi:10.1016/0012-821X(94)90082-5.

Canales, J. P., R. S. Detrick, J. Lin, J. A. Collins, and D. R. Toomey (2000), Crustal and upper mantle seismic structure beneath the rift mountains and across a nontransform offset at the Mid-Atlantic Ridge (35°N), *J. Geophys. Res.*, *105*, 2699–2719, doi:10.1029/1999JB900379.

Canales, J. P., G. Ito, R. S. Detrick, and J. Sinton (2002), Crustal thickness along the western Galapagos Spreading Center and the compensation of the Galapagos hotspot swell, *Earth Planet. Sci. Lett.*, *203*, 311–327, doi:10.1016/S0012-821X(02)00843-9.

Cande, S. C., and D. V. Kent (1995), Revised calibration of the geomagnetic polarity timescale for the Late Cretaceous and Cenozoic, *J. Geophys. Res.*, *100*, 6093–6095, doi:10.1029/94JB03098.

Cannat, M., et al. (1999), Mid-Atlantic Ridge-Azores hotspot interactions: Along-axis migration of a hotspot-derived event of enhanced magmatism 10 to 3 Ma ago, *Earth Planet. Sci. Lett.*, *173*, 257–269, doi:10.1016/S0012-821X(99)00234-4.

Chalmers, J. A., and K. H. Laursen (1995), Labrador Sea: The extent of continental and oceanic crust and the timing of the onset of seafloor spreading, *Mar. Pet. Geol.*, *12*, 205–206, doi:10.1016/0264-8172(95)92840-S.

Chen, Y. J. (1992), Oceanic crustal thickness versus spreading rate, *Geophys. Res. Lett.*, *19*, 753–756, doi:10.1029/92GL00161.

Chen, Y., and W. J. Morgan (1990), Rift valley alley transition at mid-ocean ridges, *J. Geophys. Res.*, *95*, 17,571–17,581, doi:10.1029/JB095iB11p17571/no rift v.

Chian, D. P., and K. E. Louden (1994), The continent-ocean crustal transition across the Southwest Greenland Margin, *J. Geophys. Res.*, *99*, 9117–9135, doi:10.1029/93JB03404.

Clarke, D. B. (1970), Tertiary basalts of Baffin Bay: Possible primary magma from the mantle, *Contrib. Mineral. Petrol.*, *25*, 203–224, doi:10.1007/BF00371131.

Cowie, P. A., and G. D. Karner (1990), Gravity effect of sediment compaction: Examples from the North-Sea and the Rhine Graben, *Earth Planet. Sci. Lett.*, *99*, 141–153, doi:10.1016/0012-821X(90)90078-C.

Crosby, A. G., and D. McKenzie (2009), An analysis of young ocean depth, gravity and global residual topography, *Geophys. J. Int.*, *178*, 1198–1219, doi:10.1111/j.1365-246X.2009.04224.x.

Detrick, R. S., R. P. Von Herzen, B. Parsons, D. Sandwell, and M. Dougherty (1986), Heat flow observations on the Bermuda Rise and thermal models of midplate swells, *J. Geophys. Res.*, *91*, 3701–3723, doi:10.1029/JB091iB03p03701.

Divins, D. L. (2009), NGDC Total Sediment Thickness of the World's Oceans & Marginal Seas, June 2009, http://www.ngdc.noaa.gov/mgg/sedthick/sedthick.html, Mar. Geol. and Geophys., Boulder, Colo.

Dosso, L., H. Bougault, C. Langmuir, C. Bollinger, O. Bonnier, and J. Etoubleau (1999), The age and distribution of mantle heterogeneity along the Mid-Atlantic Ridge (31°–41°N), *Earth Planet. Sci. Lett.*, *170*, 269–286, doi:10.1016/S0012-821X(99)00109-0.

Duncan, R. A. (1984), Age progressive volcanism in the New England seamounts and the opening of the central Atlantic Ocean, *J. Geophys. Res.*, *89*, 9980–9990, doi:10.1029/JB089iB12p09980.

Fedorova, T., W. R. Jacoby, and H. Wallner (2005), Crust-mantle transition and Moho model for Iceland and surroundings from seismic, topography, and gravity data, *Tectonophysics*, *396*, 119–140, doi:10.1016/j.tecto.2004.11.004.

Geldmacher, J., and K. Hoernle (2000), The 72 Ma geochemical evolution of the Madeira hotspot (eastern North Atlantic): Recycling of Paleozoic (≤500 Ma) oceanic lithosphere, *Earth Planet. Sci. Lett.*, *183*, 73–92, doi:10.1016/S0012-821X(00)00266-1.

Geldmacher, J., K. Hoernle, P. van den Bogaard, G. Zankl, and D. Garbe-Schönberg (2001), Earlier history of the ≥70-Ma-old Canary hotspot based on the temporal and geochemical evolution of the Selvagen Archipelago and neighboring seamounts in the eastern North Atlantic, *J. Volcanol. Geotherm. Res.*, *111*, 55–87, doi:10.1016/S0377-0273(01)00220-7.

Geldmacher, J., K. Hoernle, A. Klugel, P. van den Bogaard, F. Wombacher, and B. Berning (2006), Origin and geochemical evolution of the Madeira-Tore Rise (eastern North Atlantic), *J. Geophys. Res.*, *111*, B09206, doi:10.1029/2005JB003931.

Gente, P., J. Dyment, M. Maia, and J. Goslin (2003), Interaction between the Mid-Atlantic Ridge and the Azores hot spot during the last 85 Myr: Emplacement and rifting of the hot spot-derived plateaus, *Geochem. Geophys. Geosyst.*, *4*(10), 8514, doi:10.1029/2003GC000527.

Gradstein, F. M., F. P. Agterberg, J. G. Ogg, S. Hardenbol, P. Vanveen, J. Thierry, and Z. H. Huang (1994), A Mesozoic time scale, *J. Geophys. Res.*, *99*, 24,051–24,074, doi:10.1029/94JB01889.

Holm, P. M., T. Grandvuinet, J. Friis, J. R. Wilson, A. K. Barker, and S. Plesner (2008), An ^{40}Ar-^{39}Ar study of the Cape Verde hot spot: Temporal evolution in a semistationary plate environment, *J. Geophys. Res.*, *113*, B08201, doi:10.1029/2007JB005339.

Hooft, E. E. E., R. S. Detrick, D. R. Toomey, J. A. Collins, and J. Lin (2000), Crustal thickness and structure along three contrasting spreading segments of the Mid-Atlantic Ridge, 33.5°–35°N, *J. Geophys. Res.*, *105*, 8205–8226, doi:10.1029/1999JB900442.

Ito, G., and J. Lin (1995), Oceanic spreading center-hotspot interactions: Constraints from along-isochron bathymetric and gravity anomalies, *Geology*, *23*, 657–660, doi:10.1130/0091-7613(1995)023<0657:OSCHIC>2.3.CO;2.

Ito, G., J. Lin, and C. W. Gable (1996), Dynamics of mantle flow and melting at a ridge-centered hotspot: Iceland and the Mid-Atlantic Ridge, *Earth Planet. Sci. Lett.*, *144*, 53–74, doi:10.1016/0012-821X(96)00151-3.

Jaroslow, G. E., and B. E. Tucholke (1994), Mesozoic-Cenozoic sedimentation in the Kane Fracture Zone, western North Atlantic, and uplift history of the Bermuda Rise, *Geol. Soc. Am. Bull.*, *106*, 319–337, doi:10.1130/0016-7606(1994)106<0319:MCSITK>2.3.CO;2.

Klingelhöfer, F., L. Geli, L. Matias, N. Steinsland, and J. Mohr (2000), Crustal structure of a super-slow spreading centre: A seismic refraction study of Mohns Ridge, 72°N, *Geophys. J. Int.*, *141*, 509–526, doi:10.1046/j.1365-246x.2000.00098.x.

Klitgord, K. D., and H. Schouten (1986), Plate kinematics of the central Atlantic, in *The Geology of North America*, vol. M, *The Western North Atlantic Region*, edited by P. R. Vogt

and B. E. Tucholke, pp. 351–358, Geol. Soc. of Am., Boulder, Colo.

Kodaira, S., R. Mjelde, K. Gunnarsson, H. Shiobara, and H. Shimamura (1997), Crustal structure of the Kolbeinsey Ridge, North Atlantic, obtained by use of ocean bottom seismographs, *J. Geophys. Res.*, *102*, 3131–3151, doi:10.1029/96JB03487.

Kreemer, C. (2009), Absolute plate motions constrained by shear wave splitting orientations with implications for hot spot motions and mantle flow, *J. Geophys. Res.*, *114*, B10405, doi:10.1029/2009JB006416.

Kuo, B. Y., and D. W. Forsyth (1988), Gravity anomalies of the ridge-transform system in the South Atlantic between 31 and 34.5°S: Upwelling centers and variations in crustal thickness, *Mar. Geophys. Res.*, *10*, 205–232, doi:10.1007/BF00310065.

Langmuir, C., E. Klein, and T. Plank (1992), Petrological systematics of mid-ocean ridge basalts: Constraints on melt generation beneath ocean ridges, in *Mantle Flow and Melt Generation at Mid-Ocean Ridges*, *Geophys. Monogr. Ser.*, vol. 71, edited by J. Phipps Morgan et al., pp. 183–280, AGU, Washington, D. C.

Larsen, L. M., A. K. Pedersen, G. K. Pedersen, and S. Piasechi (1992), Timing and duration of early Tertiary volcanism in the North Atlantic: New evidence from West Greenland, in *Magmatism and the Causes of Continental Break-up*, edited by B. C. Storey, T. Alabaster, and R. J. Pankhurst, *Geol. Soc. Spec. Publ.*, *68*, 321–333.

Larsen, T. B., D. A. Yuen, and M. Storey (1999), Ultrafast mantle plumes and implications for flood basalt volcanism in the Northern Atlantic Region, *Tectonophysics*, *311*, 31–43, doi:10.1016/S0040-1951(99)00163-8.

Lawver, L. A., and R. D. Müller (1994), Iceland hotspot track, *Geology*, *22*, 311–314, doi:10.1130/0091-7613(1994)022<0311:IHT>2.3.CO;2.

Lin, J., and J. Phipps Morgan (1992), The spreading rate dependence of three-dimensional mid-ocean ridge gravity structure, *Geophys. Res. Lett.*, *19*, 13–16, doi:10.1029/91GL03041.

Lin, J., G. M. Purdy, H. Schouten, J. C. Sempere, and C. Zervas (1990), Evidence from gravity data for focused magmatic accretion along the Mid-Atlantic Ridge, *Nature*, *344*, 627–632, doi:10.1038/344627a0.

Louden, K. E., B. E. Tucholke, and G. N. Oakey (2004), Regional anomalies of sediment thickness, basement depth and isostatic crustal thickness in the North Atlantic Ocean, *Earth Planet. Sci. Lett.*, *224*, 193–211, doi:10.1016/j.epsl.2004.05.002.

Macdonald, K. C. (1982), Mid-ocean ridges: Fine scale tectonic, volcanic and hydrothermal processes within the plate boundary zone, *Annu. Rev. Earth Planet. Sci.*, *10*, 155–190, doi:10.1146/annurev.ea.10.050182.001103.

Magde, L. S., R. S. Detrick, and the TERA Group (1995), Crustal and upper mantle contribution to the axial gravity anomaly at the southern East Pacific Rise, *J. Geophys. Res.*, *100*, 3747–3766, doi:10.1029/94JB02869.

Marks, K. M. (1996), Resolution of the Scripps/NOAA marine gravity field from satellite altimetry, *Geophys. Res. Lett.*, *23*, 2069–2072, doi:10.1029/96GL02059.

Minshull, T. A., R. S. White, J. C. Mutter, P. Buhl, R. S. Detrick, C. A. Williams, and E. Morris (1991), Crustal structure at the Blake Spur Fracture Zone from expanding spread profiles, *J. Geophys. Res.*, *96*, 9955–9984, doi:10.1029/91JB00431.

Müller, R. D., J. Y. Royer, and L. A. Lawver (1993), Revised plate motions relative to the hotspots from combined Atlantic and Indian Ocean hotspot tracks, *Geology*, *21*, 275–278, doi:10.1130/0091-7613(1993)021<0275:RPMRTT>2.3.CO;2.

Müller, R. D., M. Sdrolias, C. Gaina, and W. R. Roest (2008), Age, spreading rates, and spreading asymmetry of the world's ocean crust, *Geochem. Geophys. Geosyst.*, *9*, Q04006, doi:10.1029/2007GC001743.

Neumann, G. A., D. W. Forsyth, and D. Sandwell (1993), Comparison of marine gravity from shipboard and high-density satellite altimetry along the Mid-Atlantic Ridge, 30.5°–35.5°S, *Geophys. Res. Lett.*, *20*, 1639–1642, doi:10.1029/93GL01487.

Noble, R. H., R. M. Macintyre, and P. E. Brown (1988), Age constraints on Atlantic evolution: Timing of magmatic activity along the E Greenland continental margin, in *Early Tertiary Volcanism and the Opening of the NE Atlantic*, edited by A. C. Morton and L. M. Parson, *Geol. Soc. Spec. Publ.*, *39*, 201–214.

Norton, I. O. (2000), Global hotspot reference frames and plate motion, in *The History and Dynamics of Global Plate Motions*, *Geophys. Monogr. Ser.*, vol. 121, edited by M. A. Richards, R. G. Gordon, and R. D. van der Hilst, pp. 339–357, AGU, Washington, D. C.

Parker, R. L. (1972), The rapid calculation of potential anomalies, *Geophys. J. R. Astron. Soc.*, *31*, 447–455.

Pe-Piper, G., A. de Jong, D. J. W. Piper, and L. F. Jansa (2006), Morphology, petrography, age and origin of the Fogo seamounts, eastern Canada, *Open File 5182*, 74 pp., Geol. Surv. of Can., Ottawa.

Pe-Piper, G., D. J. W. Piper, L. F. Jansa, and A. de Jonge (2007), Early cretaceous opening of the North Atlantic Ocean: Implications of the petrology and tectonic setting of the Fogo seamounts off the SW Grand Banks, Newfoundland, *Geol. Soc. Am. Bull.*, *119*, 712–724, doi:10.1130/B26008.1.

Pollitz, F. F. (1991), Two-stage model of African absolute motion during the Last 30 million years, *Tectonophysics*, *194*, 91–106, doi:10.1016/0040-1951(91)90274-V.

Reid, I., and H. R. Jackson (1981), Oceanic spreading rate and crustal thickness, *Mar. Geophys. Res.*, *5*, 165–172.

Roest, W. R., and S. P. Srivastava (1989), Sea-floor spreading in the Labrador Sea: A new reconstruction, *Geology*, *17*, 1000–1003, doi:10.1130/0091-7613(1989)017<1000:SFSITL>2.3.CO;2.

Rovere, M., C. R. Ranero, R. Sartori, L. Torelli, and N. Zitellini (2004), Seismic images and magnetic signature of the Late Jurassic to Early Cretaceous Africa-Eurasia plate boundary off SW Iberia, *Geophys. J. Int.*, *158*, 554–568, doi:10.1111/j.1365-246X.2004.02339.x.

Ruedas, T., and H. Schmeling (2008), Kinematic models for the thickness of oceanic crust at and near mid-oceanic spreading centers, *J. Geophys. Res.*, *113*, B01402, doi:10.1029/2006JB004746.

Sandwell, D. T., and W. H. F. Smith (2009), Global marine gravity from retracked Geosat and ERS-1 altimetry: Ridge segmentation versus spreading rate, *J. Geophys. Res.*, *114*, B01411, doi:10.1029/2008JB006008.

Schilling, J.-G. (1973), Iceland mantle plume: Geochemical study of Reykjanes Ridge, *Nature*, *242*, 565–571, doi:10.1038/242565a0.

Schilling, J.-G. (1975), Azores mantle blob: Rare-earth evidence, *Earth Planet. Sci. Lett.*, *25*, 103–115, doi:10.1016/0012-821X(75)90186-7.

Schilling, J.-G. (1985), Upper mantle heterogeneities and dynamics, *Nature*, *314*, 62–67, doi:10.1038/314062a0.

Schilling, J.-G. (1991), Fluxes and excess temperatures of mantle plumes inferred from their interaction with migrating mid-ocean ridges, *Nature*, *352*, 397–403, doi:10.1038/352397a0.

Schilling, J.-G., M. Zajac, R. Evans, T. Johnston, W. White, J. D. Devine, and R. Kingsley (1983), Petrologic and geochemical variations along the Mid-Atlantic Ridge from 29°N to 73°N, *Am. J. Sci.*, *283*, 510–586, doi:10.2475/ajs.283.6.510.

Schilling, J.-G., B. B. Hanan, B. Mccully, R. H. Kingsley, and D. Fontignie (1994), Influence of the Sierra-Leone mantle plume on the equatorial Mid-Atlantic Ridge: A Nd-Sr-Pb isotopic study, *J. Geophys. Res.*, *99*, 12,005–12,028, doi:10.1029/94JB00337.

Searle, R. C. (1976), Lithospheric structure of Azores Plateau from Rayleigh-wave dispersion, *Geophys. J. R. Astron. Soc.*, *44*, 537–546.

Shaw, P. R., and J. Lin (1993), Causes and consequences of variations in faulting style at the Mid-Atlantic Ridge, *J. Geophys. Res.*, *98*, 21,839–21,851, doi:10.1029/93JB01565.

Silveira, G., E. Stutzmann, A. Davaille, J. P. Montagner, L. Mendes-Victor, and A. Sebai (2006), Azores hotspot signature in the upper mantle, *J. Volcanol. Geotherm. Res.*, *156*, 23–34, doi:10.1016/j.jvolgeores.2006.03.022.

Smith, W. H. F., and D. T. Sandwell (1997), Global sea floor topography from satellite altimetry and ship depth soundings, *Science*, *277*, 1956–1962, doi:10.1126/science.277.5334.1956.

Srivastava, S. P., and W. R. Roest (1992), Kings Trough: Reactivated pseudo-fault of a propagating rift, *Geophys. J. Int.*, *108*, 143–150, doi:10.1111/j.1365-246X.1992.tb00845.x.

Srivastava, S. P., and C. R. Tapscott (1986), Plate kinematics of the North Atlantic, in *The Geology of North America*, vol. M, *The Western North Atlantic Region*, edited by P. R. Vogt and B. E. Tucholke, pp. 379–404, Geol. Soc. of Am., Boulder, Colo.

Srivastava, S. P., H. Schouten, W. R. Roest, K. D. Klitgord, L. C. Kovacs, J. Verhoef, and R. Macnab (1990), Iberian plate kinematics: A jumping plate boundary between Eurasia and Africa, *Nature*, *344*, 756–759, doi:10.1038/344756a0.

Sullivan, K. D., and C. E. Keen (1977), Newfoundland seamounts: Petrology and geochemistry, *Geol. Assoc. Can. Spec. Pap.*, *16*, 461–476.

Thibaud, R., P. Gente, and M. Maia (1998), A systematic analysis of the Mid-Atlantic Ridge morphology and gravity between 15°N and 40°N: Constraints of the thermal structure, *J. Geophys. Res.*, *103*, 24,223–24,243, doi:10.1029/97JB02934.

Tolstoy, M., A. J. Harding, and J. A. Orcutt (1993), Crustal thickness on the Mid-Atlantic Ridge: Bull's-eye gravity anomalies and focused accretion, *Science*, *262*, 726–729, doi:10.1126/science.262.5134.726.

Tucholke, B. E., and W. J. Ludwig (1982), Structure and origin of the J Anomaly Ridge, western North Atlantic Ocean, *J. Geophys. Res.*, *87*, 9389–9407, doi:10.1029/JB087iB11p09389.

Tucholke, B. E., and J.-C. Sibuet (2007), Leg 210 synthesis: Tectonic, magmatic, and sedimentary evolution of the Newfoundland-Iberia rift, *Proc. Ocean Drill. Program Sci. Results*, *210*, 1–56.

Tucholke, B. E., and N. C. Smoot (1990), Evidence for age and evolution of Corner seamounts and Great Meteor Seamount chain from multibeam bathymetry, *J. Geophys. Res.*, *95*, 17,555–17,569, doi:10.1029/JB095iB11p17555.

Tucholke, B. E., and P. R. Vogt (1979), Western North Atlantic: Sedimentary evolution and aspects of tectonic history, *Initial Rep. Deep Sea Drill. Proj.*, *43*, 791–825.

Tucholke, B. E., et al. (1979), Site 384: The Cretaceous/Tertiary boundary, Aptian reefs, and the J-Anomaly Ridge, *Initial Rep. Deep Sea Drill. Proj.*, *43*, 107–165.

Tucholke, B. E., D. S. Sawyer, and J.-C. Sibuet (2007), Breakup of the Newfoundland-Iberia rift, in *Imaging, Mapping and Modelling Continental Lithosphere Extension and Breakup*, edited by G. D. Karner, G. Manatschal, and L. M. Pinheiro, *Geol. Soc. Spec. Publ.*, *282*, 9–46, doi:10.1144/SP282.2.

Turcotte, D. L., and G. Schubert (2002), *Geodynamics*, 2nd ed., 472 pp., Cambridge Univ. Press, Cambridge, U. K.

Vogt, P. R. (1976), Plumes, subaxial pipe-flow, and topography along the Mid-Oceanic Ridge, *Earth Planet. Sci. Lett.*, *29*, 309–325, doi:10.1016/0012-821X(76)90135-7.

Vogt, P. R. (1991), Bermuda and Appalachian-Labrador rises: Common non-hotspot processes?, *Geology*, *19*, 41–44, doi:10.1130/0091-7613(1991)019<0041:BAALRC>2.3.CO;2.

Vogt, P. R., and W. Y. Jung (2005), Paired basement ridges: Spreading axis migration across mantle heterogeneities?, *Spec. Pap. Geol. Soc. Am.*, *388*, 555–579.

Vogt, P. R., and W. Y. Jung (2007), Origin of the Bermuda volcanoes and the Bermuda Rise: History, observations, models, and puzzles, *Spec. Pap. Geol. Soc. Am.*, *430*, 553–591.

Weir, N. R. W., R. S. White, B. Brandsdottir, P. Einarsson, H. Shimamura, H. Shiobara, and R. F. Team (2001), Crustal structure of the northern Reykjanes Ridge and Reykjanes Peninsula, southwest Iceland, *J. Geophys. Res.*, *106*, 6347–6368, doi:10.1029/2000JB900358.

Wessel, P., and W. H. F. Smith (1998), New, improved version of Generic Mapping Tools released, *Eos Trans. AGU*, *79*(47), 579, doi:10.1029/98EO00426.

White, R., and D. McKenzie (1989), Magmatism at rift zones: The generation of volcanic continental margins and flood basalts, *J. Geophys. Res.*, *94*, 7685–7729, doi:10.1029/JB094iB06p07685.

White, R. S., T. A. Minshull, M. J. Bickle, and C. J. Robinson (2001), Melt generation at very slow-spreading oceanic ridges: Constraints from geochemical and geophysical data, *J. Petrol.*, *42*, 1171–1196, doi:10.1093/petrology/42.6.1171.

Whitmarsh, R. B., A. Ginzburg, and R. C. Searle (1982), The structure and origin of the Azores-Biscay Rise, North-east Atlantic Ocean, *Geophys. J. R. Astron. Soc.*, *70*, 79–107.

Williams, C. A. (1975), Sea-floor spreading in Bay of Biscay and its relationship to the North Atlantic, *Earth Planet. Sci. Lett.*, *24*, 440–456, doi:10.1016/0012-821X(75)90151-X.

Wolfe, C. J., I. T. Bjarnason, J. C. VanDecar, and S. C. Solomon (1997), Seismic structure of the Iceland mantle plume, *Nature*, *385*, 245–247, doi:10.1038/385245a0.

Yu, D. M., D. Fontignie, and J. G. Schilling (1997), Mantle plume-ridge interactions in the central North Atlantic: A Nd isotope study of Mid-Atlantic Ridge basalts from 30°N to 50°N, *Earth Planet. Sci. Lett.*, *146*, 259–272, doi:10.1016/S0012-821X(96)00221-X.

Zhang, Y. S., and T. Tanimoto (1992), Ridges, hotspots and their interaction as observed in seismic velocity maps, *Nature*, *355*, 45–49, doi:10.1038/355045a0.

Zhao, D. (2001), Seismic structure and origin of hotspots and mantle plumes, *Earth Planet. Sci. Lett.*, *192*, 251–265, doi:10.1016/S0012-821X(01)00465-4.

GEOCHEMISTRY GEOPHYSICS GEOSYSTEMS, VOL. 12, Q0AE02, 25 PP., 2011
doi:10.1029/2010GC003402

Auxiliary Material

Auxiliary material for this article contains the comparison of the gravity effects of lithosphere cooling and MBA, the comparison of the gravity-derived crustal thickness with seismic refractory profiles.

Auxiliary material files may require downloading to a local drive depending on platform, browser, configuration, and size. To open auxiliary materials in a browser, click on the label. To download, Right-click and select “Save Target As…” (PC) or CTRL-click and select “Download Link to Disk” (Mac).

Additional file information is provided in the readme.txt.

Figure S1

Size: 294 KB
Format: PDF
Caption: Locations of 18 MBA gravity profiles (white lines) illustrated in Figure S2, plotted on a map of calculated gravity effects of lithospheric cooling.

Figure S2

Size: 112 KB
Format: PDF
Caption: Comparison of the calculated gravity effects of lithospheric cooling and MBA along the 18 profiles shown in Figure S1.

Figure S3

Size: 1.1 MB
Format: PDF
Caption: Comparison of seismic refraction profiles with our gravity-derived crustal thickness.

Citation: Wang, T., J. Lin, B. Tucholke, and Y. J. Chen (2011), Crustal thickness anomalies in the North Atlantic Ocean basin from gravity analysis, *Geochem. Geophys. Geosyst.*, *12*, Q0AE02, doi:10.1029/2010GC003402.

Auxiliary Material for Paper 2010GC003402

Crustal thickness anomalies in the North Atlantic Ocean basin from gravity analysis

Tingting Wang
Institute of Theoretical and Applied Geophysics, School of Earth and Space Sciences, Peking University, Beijing, China

Jian Lin and Brian Tucholke
Department of Geology and Geophysics, Woods Hole Oceanographic Institution, Woods Hole, Massachusetts, USA

Yongshun John Chen
Institute of Theoretical and Applied Geophysics, School of Earth and Space Sciences, Peking University, Beijing, China

Wang, T., J. Lin, B. Tucholke, and Y. J. Chen (2011), Crustal thickness anomalies in the North Atlantic Ocean basin from
gravity analysis, Geochem. Geophys. Geosyst., 12, Q0AE02,
doi:10.1029/2010GC003402.

Introduction

The auxiliary material contains the comparison of the gravity effects of lithosphere cooling and MBA, the comparison of the gravity-derived
crustal thickness with seismic refractory profiles.

1. 2010gc003402-fs01.pdf
Figure S1. Locations of 18 MBA gravity profiles (white lines) illustrated in Figure S2, plotted on a map of calculated gravity effects of lithospheric cooling.

2. 2010gc003402-fs02.pdf
Figure S2. Comparison of the calculated gravity effects of lithospheric cooling (red line) and MBA (black line) along the 18 profiles shown in Figure S1.

3. 2010gc003402-fs03.pdf
Figure S3. Comparison of seismic refraction profiles with our gravity-derived crustal thickness. Depths of the seafloor, basement, and Moho as determined
in the seismic profiles are shown as purple, light blue, and black solid lines, respectively;

Moho is assumed to be at 7.9-8.0 km s-1 unless otherwise indicated.
Seafloor and basement depths from the dataset used in this study are shown as purple and light blue dashed lines, respectively. Moho depths from our best fitting gravity-derived crustal thickness model (with crustal density of 2700 kg m-3) are shown as red solid lines. Moho depths from our models that used other assumed crustal densities are also shown along several profiles. References for profiles: (1) Whitmarsh and Calvert [1986]; (2), (3), and (4) Hooft et al. [2000];
(5) Canales et al. [2000]; (6) Purdy and Detrick [1986]; (7) Detrick and Purdy [1980]; (8) Korenaga et al. [2000]; (9) Hopper et al. [2003]; (10) Holbrook et al. [2001];
(11) Funck et al. [2007]; (12) Funck et al. [2003]; (13) Van Avendonk et al. [2006]; (14) Lau et al. [2006]; (15) Funck et al. [2004]; (16) Wu et al. [2006];
(17) Lizarralde et al. [2004]; (18) Morris et al. [1993]; (19) Minshull et al. [1991];(20) Bunce et al. [1969]; (21) Bohnhoff and Makris [2004]; (22) White and Smith [2009];
(23) Barton and White [1997]; (24) Bullock and Minshull [2005]; (25) Ginzburg et al. [1985];(26) Whitmarsh et al. [1982]; (27) and (28) Whitmarsh et al. [1996]; (29) Dean et al. [2000];
(30) Whitmarsh et al. [1990]; (31) Afilhado et al. [2008]; (32) and (33) Klingelhoefer et al. [2009].

References not in the main text are as follows:

Afilhado, A., L. Matias, H. Shiobara, A. Hirn, L. Mendes-Victor, and H. Shimamura (2008), From unthinned continent to ocean: The deep structure of the West Iberia passive continental margin at 38 deg. N, Tectonophys., 458, 9-50, doi:10.1016/j.tecto.2008.03.002.

Barton, A. J., and R. S. White (1997), Crustal structure of Edoras Bank continental margin and mantle thermal anomalies beneath the North Atlantic, J. Geophys. Res., 102, 3109-3129, doi:10.1029/96JB03387.

Bohnhoff, M., and J. Makris (2004), Crustal structure of the southeastern Iceland-Faeroe Ridge (IFR) from wide aperture seismic data, J. Geodyn., 37, 233-252, doi:10.1016/j.jog.2004.02.004.

Bullock, A. D., and T. A. Minshull (2005), From continental extension to seafloor spreading: Crustal structure of the Goban Spur rifted margin, southwest of the UK, Geophys. J. Int., 163, 527-546, doi:10.1111/j.1365-246X.2005.02726.x.

Bunce, E. T., D. A. Fahlquist, and J. W. Clough (1969), Seismic refraction and reflection measurements-Puerto Rico Outer Ridge, J. Geophys. Res., 74, 3082-3094,

doi:10.1029/JB074i012p03082.

Canales, J. P., J. A. Collins, J. Escartin, and R. S. Detrick (2000), Seismic structure across the rift valley of the Mid-Atlantic Ridge at 23 deg. 20' (MARK area): Implications for crustal
accretion processes at slow spreading ridges, J. Geophys. Res., 105, 28,411-28,425, doi:10.1029/2000JB900301.

Dean, S. M., T. A. Minshull, R. B. Whitmarsh, and K. E. Louden (2000), Deep structure of the ocean-continent transition in the southern Iberia Abyssal Plain from seismic refraction profiles: The IAM-9 transect at 40 deg. 20'N, J. Geophys. Res., 105, 5859-5885, doi:10.1029/1999JB900301.

Detrick, R. S., and G. M. Purdy (1980), The crustal structure of the Kane Fracture Zone from seismic refraction studies, J. Geophys. Res., 85, 3759-3777, doi:10.1029/JB085iB07p03759.

Funck, T., J. R. Hopper, H. C. Larsen, K. E. Louden, B. E. Tucholke, and W. S. Holbrook (2003), Crustal structure of the ocean-continent transition at Flemish Cap: Seismic refraction results,
J. Geophys. Res., 108, 2531, doi:10.1029/2003JB002434.

Funck, T., H. R. Jackson, K. E. Louden, S. A. Dehler, and Y. Wu (2004), Crustal structure of the northern Nova Scotia rifted continental margin (eastern Canada), J. Geophys. Res., 109, B09102, doi:10.1029/2004JB003008.

Funck, T., H. R. Jackson, K. E. Louden, and F. Klingelhofer (2007), Seismic study of the transform-rifted margin in Davis Strait between Baffin Island (Canada) and Greenland: What
happens when a plume meets a transform, J. Geophys. Res., 112, B04402, doi:10.1029/2006JB004308.

Ginzburg, A., R. B. Whitmarsh, D. G. Roberts, L. Montadert, A. Camus, and F. Avedik (1985), The deep seismic structure of the northern continental margin of the Bay of Biscay, Ann. Geophys., 3, 499-510.

Holbrook, W. S., et al. (2001), Mantle thermal structure and active upwelling during continental breakup in the North Atlantic, Earth Planet. Sci. Lett., 190, 251-266, doi:10.1016/S0012-821X(01)00392-2.

Hopper, J. R., T. Dahl-Jensen, W. S. Holbrook, H. C. Larsen, D. Lizarralde, J. Korenaga, G. M. Kent, and P. B. Kelemen (2003), Structure of the SE Greenland margin from seismic reflection
and refraction data: Implications for nascent spreading center subsidence and asymmetric crustal accretion during North Atlantic opening, J. Geophys. Res., 108, 2269, doi:10.1029/2002JB001996.

Klingelhoefer, F., C. Labails, E. Cosquer, S. Rouzo, L. Geli, D. Aslanian, J. L. Olivet, M. Sahabi, H. Nouze, and P. Unternehr (2009), Crustal structure of the SW-Moroccan margin from wide-angle and reflection seismic data (the DAKHLA experiment) Part A: Wide-angle seismic models,
Tectonophys., 468, 63-82, doi:10.1016/j.tecto.2008.07.022.

Korenaga, J., W. S. Holbrook, G. M. Kent, P. B. Kelemen, R. S. Detrick, H. C. Larsen, J. R. Hopper, and T. Dahl-Jensen (2000), Crustal structure of the southeast Greenland margin from
joint refraction and reflection seismic tomography, J. Geophys. Res., 105, 21,591-21,614, doi:10.1029/2000JB900188.

Lau, K. W. H., K. E. Louden, S. Deemer, J. Hall, J. R. Hopper, B. E. Tucholke, W. S. Holbrook, and H. C. Larsen (2006), Crustal structure across the Grand Banks-Newfoundland Basin continental margin-I. Results
from a seismic reflection profile, Geophys. J. Int., 167, 157-170, doi:10.1111/j.1365-246X.2006.02989.x.

Lizarralde, D., J. B. Gaherty, J. A. Collins, G. Hirth, and S. D. Kim (2004), Spreading-rate dependence of melt extraction at mid-ocean ridges from mantle seismic refraction data, Nature, 432, 744-747, doi:10.1038/nature03140.

Morris, E., R. S. Detrick, T. A. Minshull, J. C. Mutter, R. S. White, W. S. Su, and P. Buhl (1993), Seismic structure of oceanic crust in the western North Atlantic, J. Geophys. Res., 98, 13,879-13,903, doi:10.1029/93JB00557.

Purdy, G. M., and R. S. Detrick (1986), Crustal structure of the mid-Atlantic Ridge at 23 deg. N from seismic refraction studies, J. Geophys. Res., 91, 3739-3762, doi:10.1029/JB091iB03p03739

Van Avendonk, H. J. A., W. S. Holbrook, G. T. Nunes, D. J. Shillington, B. E. Tucholke, K. E. Louden, H. C. Larsen, and J. R. Hopper (2006), Seismic velocity structure of the rifted margin

of the eastern Grand Banks of Newfoundland, Canada, J. Geophys. Res., 111, B11404, doi:10.1029/2005JB004156.

White, R. S., and L. K. Smith (2009), Crustal structure of the Hatton and the conjugate east Greenland rifted volcanic continental margins, NE Atlantic, J. Geophys. Res., 114, B02305, doi:10.1029/2008JB005856.

Whitmarsh, R. B., and A. J. Calvert (1986), Crustal structure of Atlantic fracture zones-I. The Charlie-Gibbs Fracture Zone, Geophys. J. R. Astron. Soc., 85, 107-138.

Whitmarsh, R. B., P. R. Miles, and A. Mauffret (1990), The ocean-continent boundary off the western continental margin of Iberia-I. Crustal structure at 40 deg. 30'N, Geophys. J. Int., 103, 509-531, doi:10.1111/j.1365-246X.1990.tb01788.x.

Whitmarsh, R. B., R. S. White, S. J. Horsefield, J. C. Sibuet, M. Recq, and V. Louvel (1996), The ocean-continent boundary off the western continental margin of Iberia: Crustal structure west of Galicia Bank, J. Geophys. Res., 101, 28,291-28,314, doi:10.1029/96JB02579.

Wu, Y., K. E. Louden, T. Funck, H. R. Jackson, and S. A. Dehler (2006), Crustal structure of the central Nova Scotia margin off Eastern Canada, Geophys. J. Int., 166, 878-906, doi:10.1111/j.1365-246X.2006.02991.x.

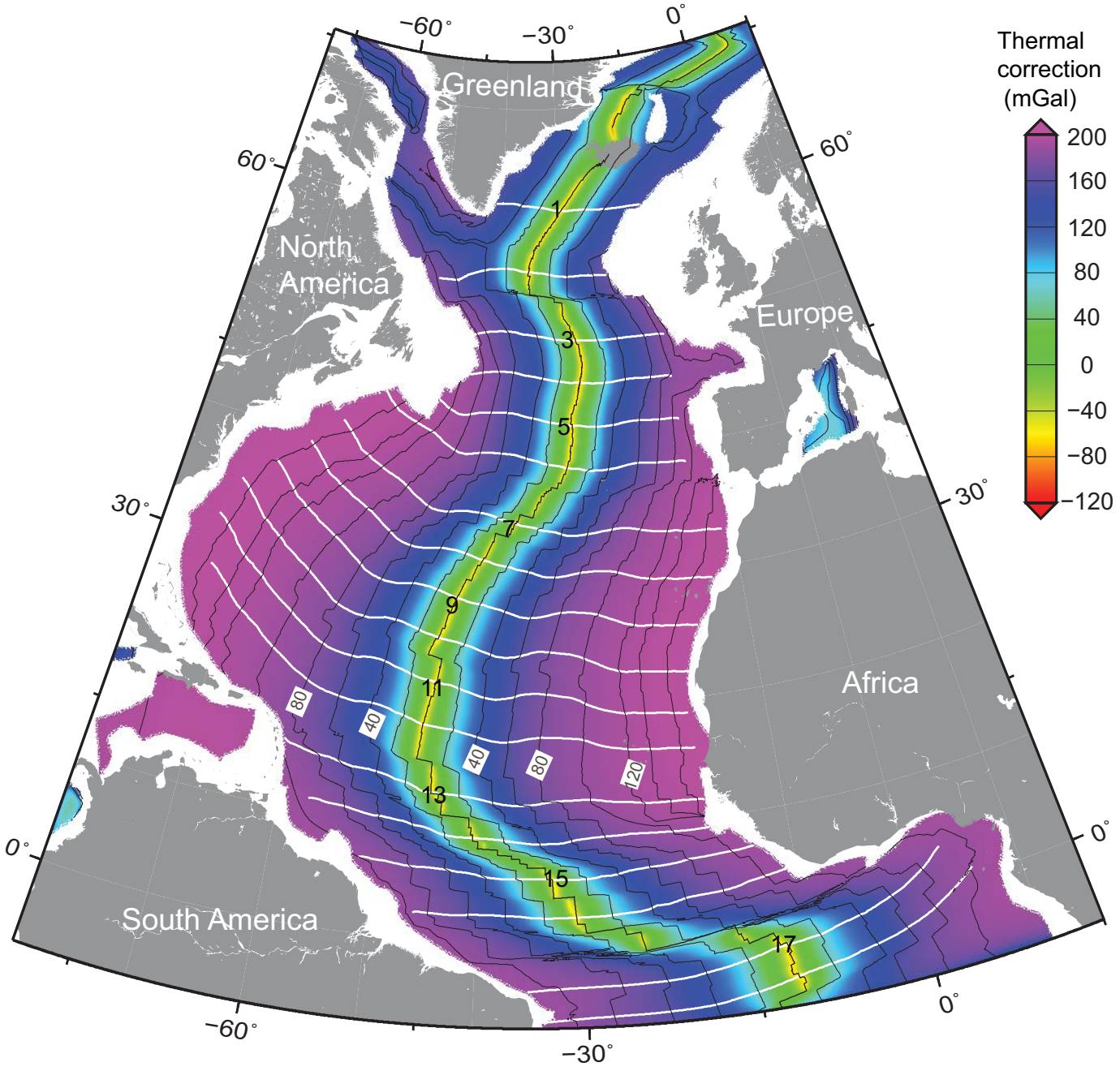
Thermal correction (mGal)
200
160
120
80
40
0
−40
−80
−120
Greenland
North America
Europe
Africa
South America
−60°
−30°
0°
60°
30°
1
3
5
7
9
11
13
15
17
80
40
40
80
120

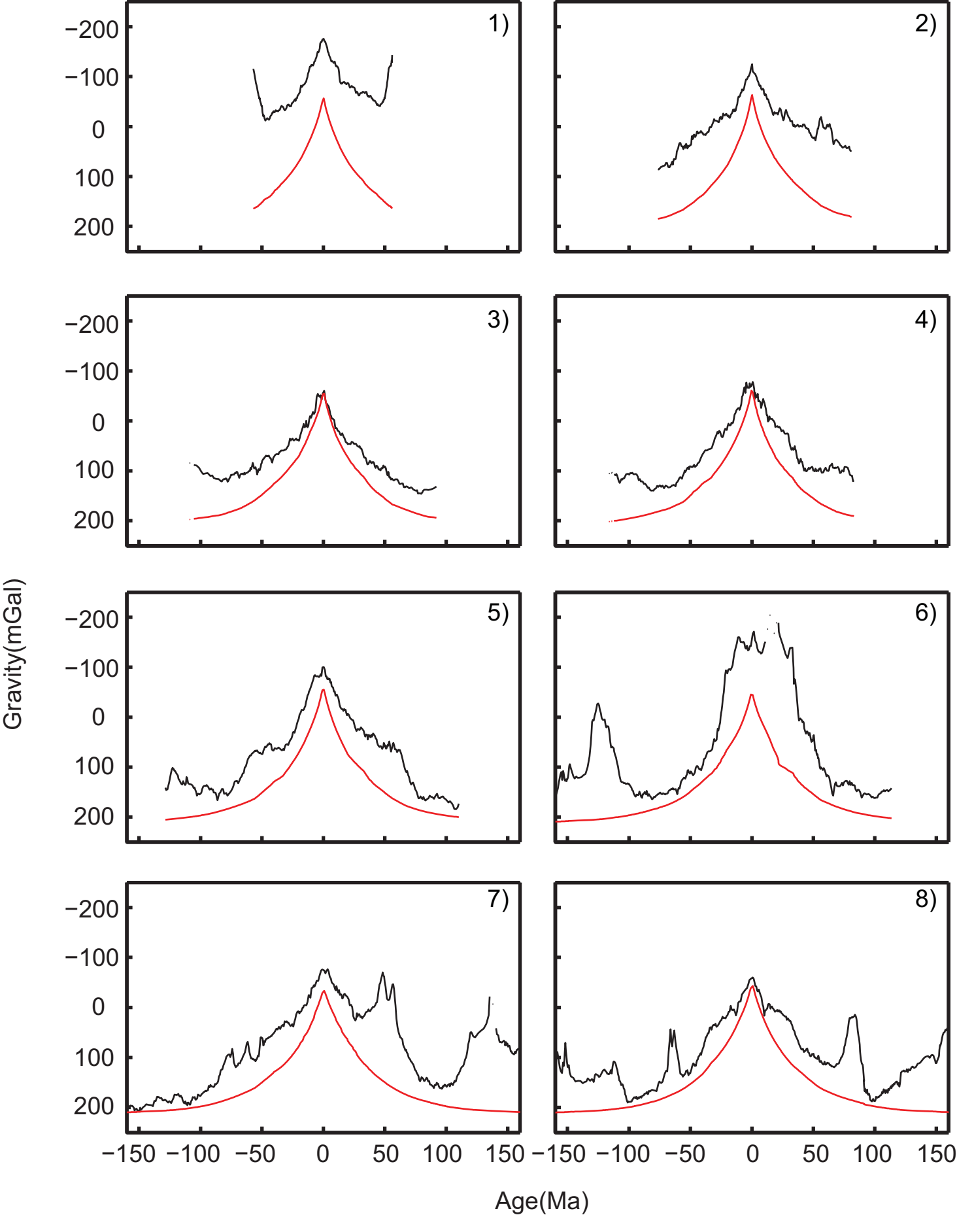
1)
2)
3)
4)
5)
6)
7)
8)
−200
−100
0
100
200
Gravity(mGal)
−150
−100
−50
0
50
100
150
Age(Ma)

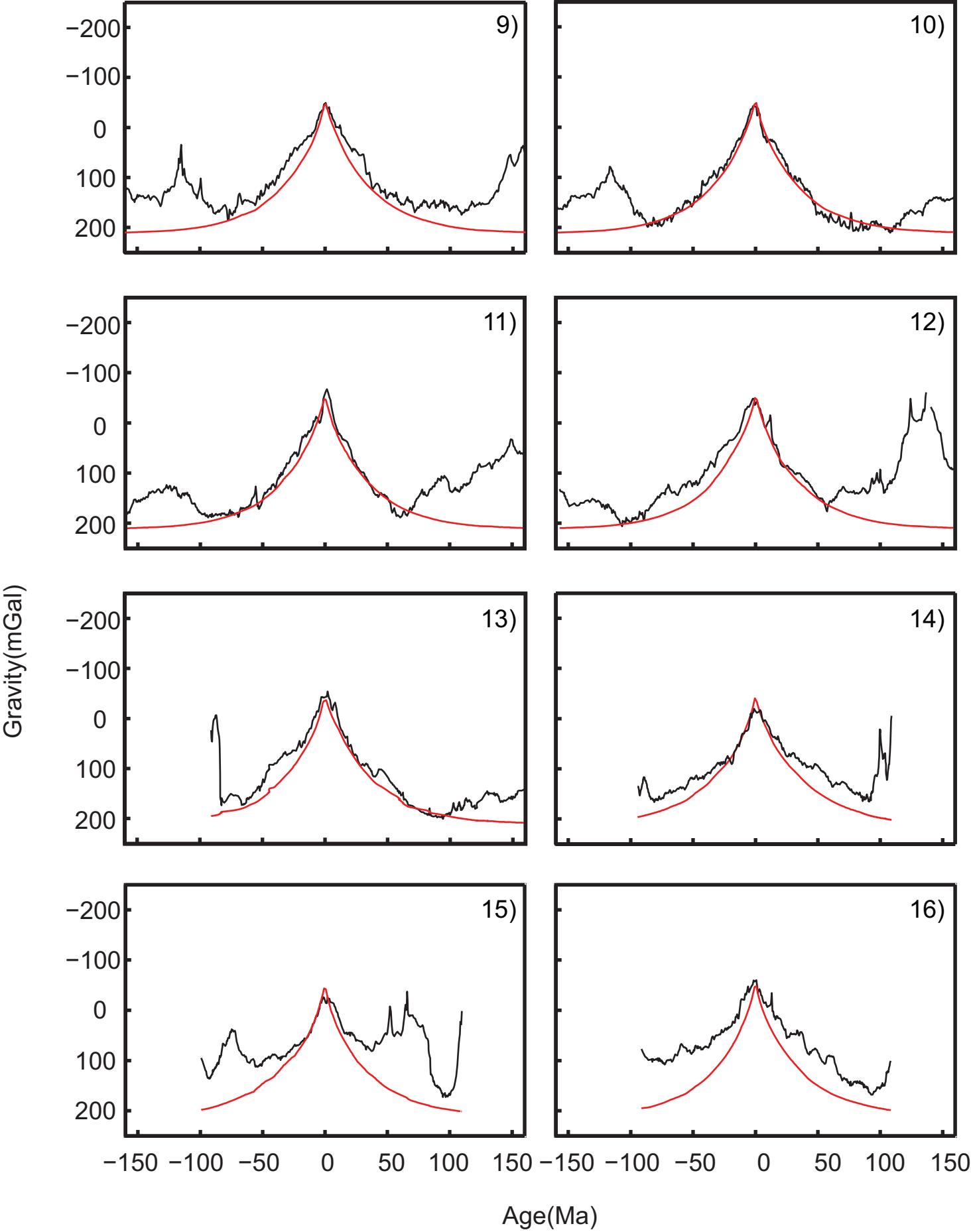
9)
10)
11)
12)
13)
14)
15)
16)
−200
−100
0
100
200
Gravity(mGal)
−150
−100
−50
0
50
100
150
Age(Ma)

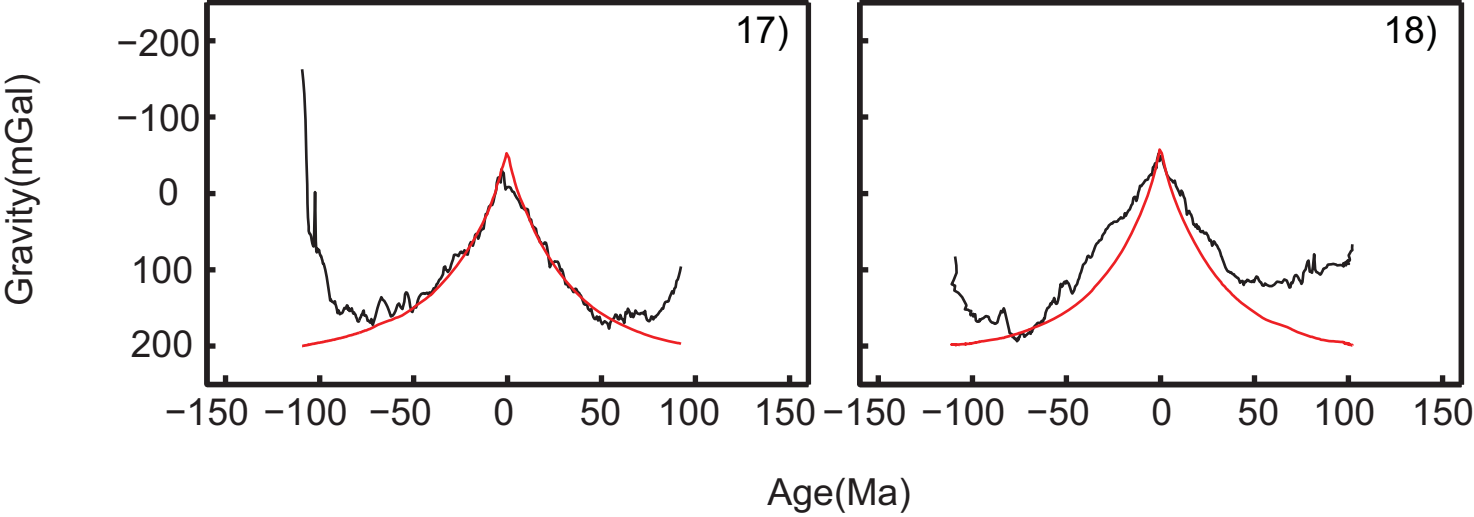
17)
18)
−200
−100
0
100
200
Gravity(mGal)
−150 −100 −50 0 50 100 150
−150 −100 −50 0 50 100 150
Age(Ma)

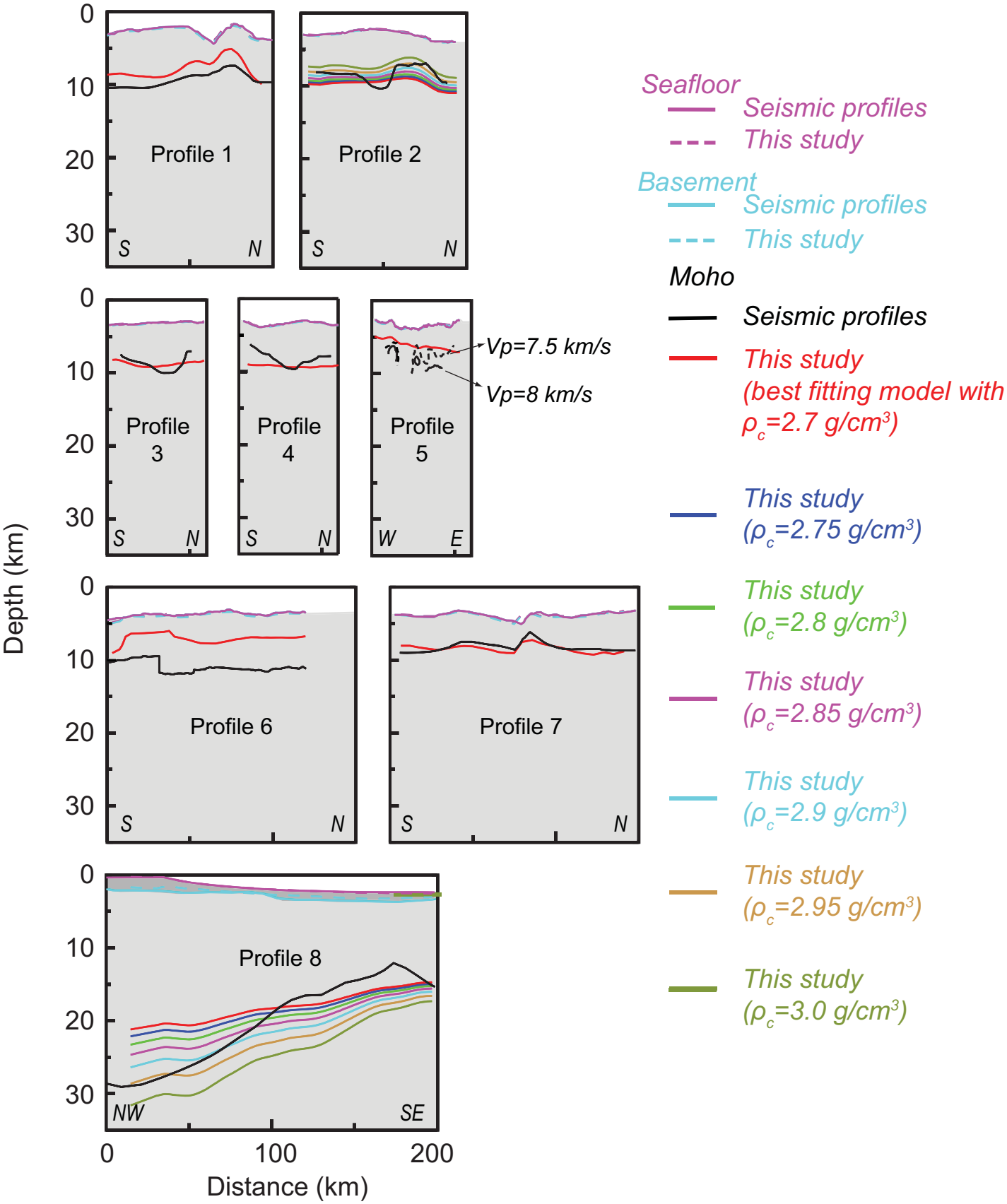
Profile 1
Profile 2
Profile 3
Profile 4
Profile 5
Profile 6
Profile 7
Profile 8
S
N
W
E
NW
SE
Vp=7.5 km/s
Vp=8 km/s
Depth (km)
0
10
20
30
0
100
200
Distance (km)
Seafloor
Seismic profiles
This study
Basement
Seismic profiles
This study
Moho
Seismic profiles
This study
(best fitting model with
ρc=2.7 g/cm3)
This study
(ρc=2.75 g/cm3)
This study
(ρc=2.8 g/cm3)
This study
(ρc=2.85 g/cm3)
This study
(ρc=2.9 g/cm3)
This study
(ρc=2.95 g/cm3)
This study
(ρc=3.0 g/cm3)

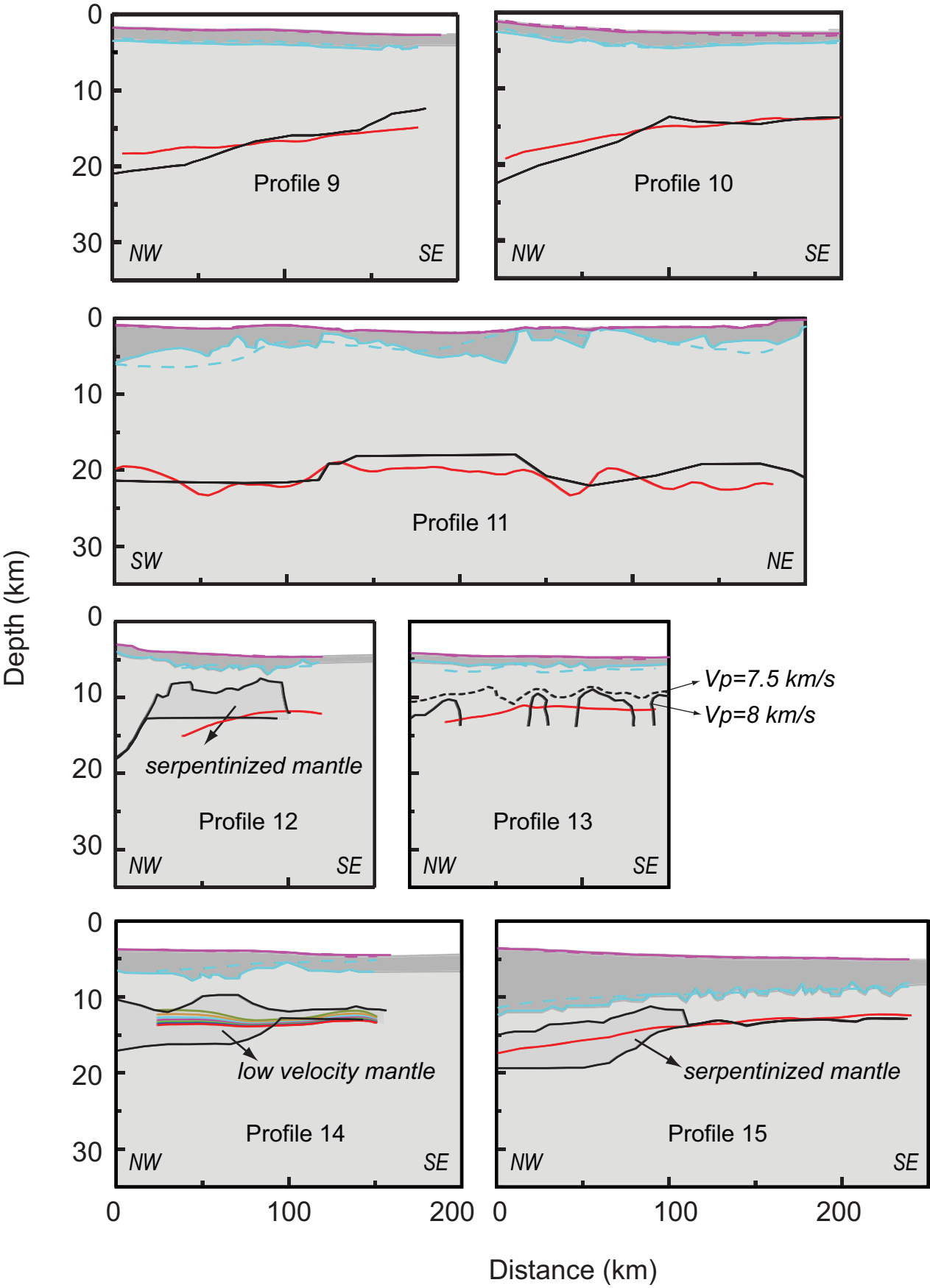
Depth (km)
0
10
20
30
Profile 9
NW
SE
Profile 10
NW
SE
Profile 11
SW
NE
serpentinized mantle
Profile 12
NW
SE
Profile 13
NW
SE
Vp=7.5 km/s
Vp=8 km/s
low velocity mantle
Profile 14
NW
SE
serpentinized mantle
Profile 15
NW
SE
0
100
200
Distance (km)

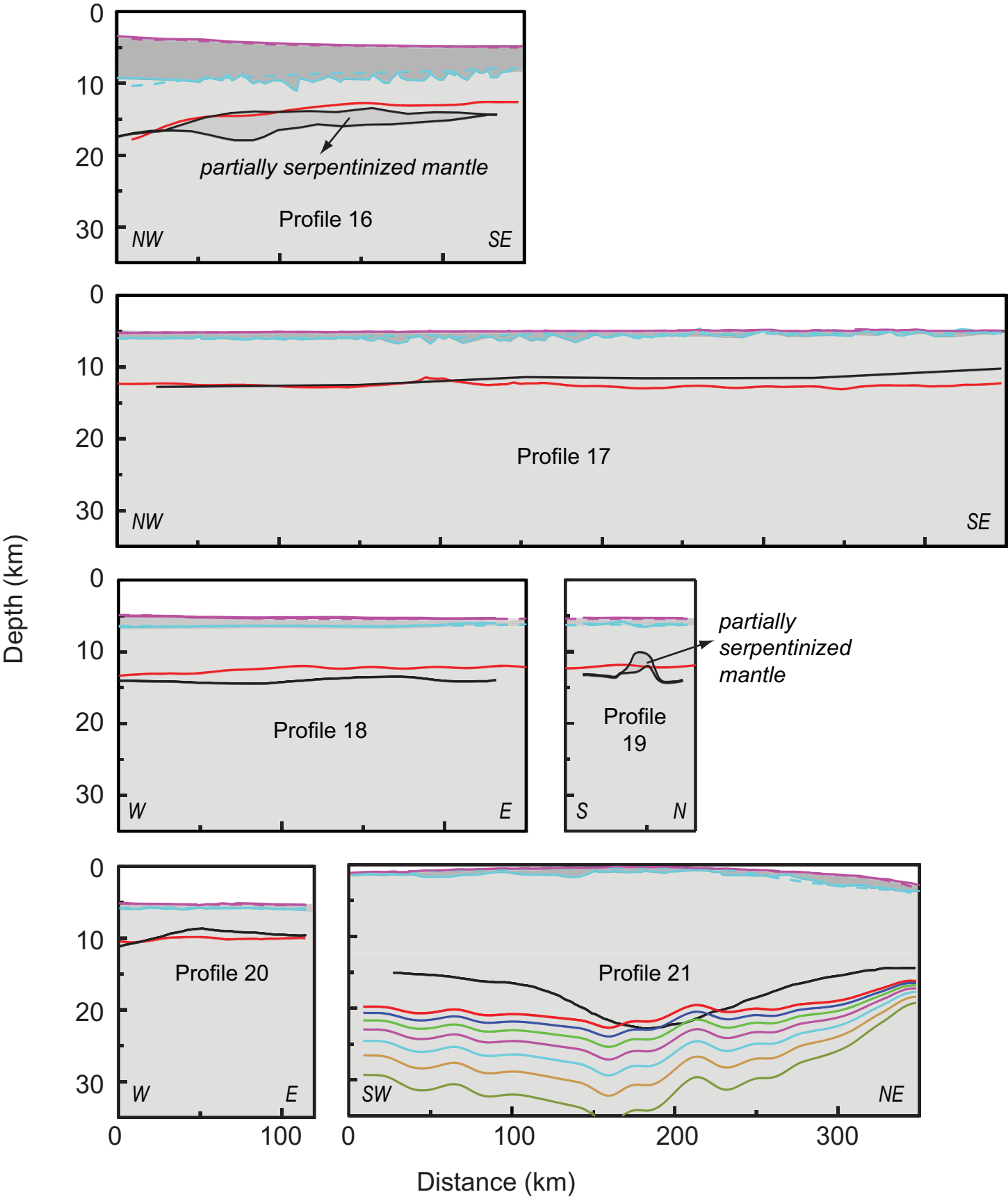
0
10
20
30
partially serpentinized mantle
Profile 16
NW
SE
Profile 17
Profile 18
W
E
Profile
19
S
N
partially
serpentinized
mantle
Profile 20
Profile 21
SW
NE
Depth (km)
0
100
200
300
Distance (km)

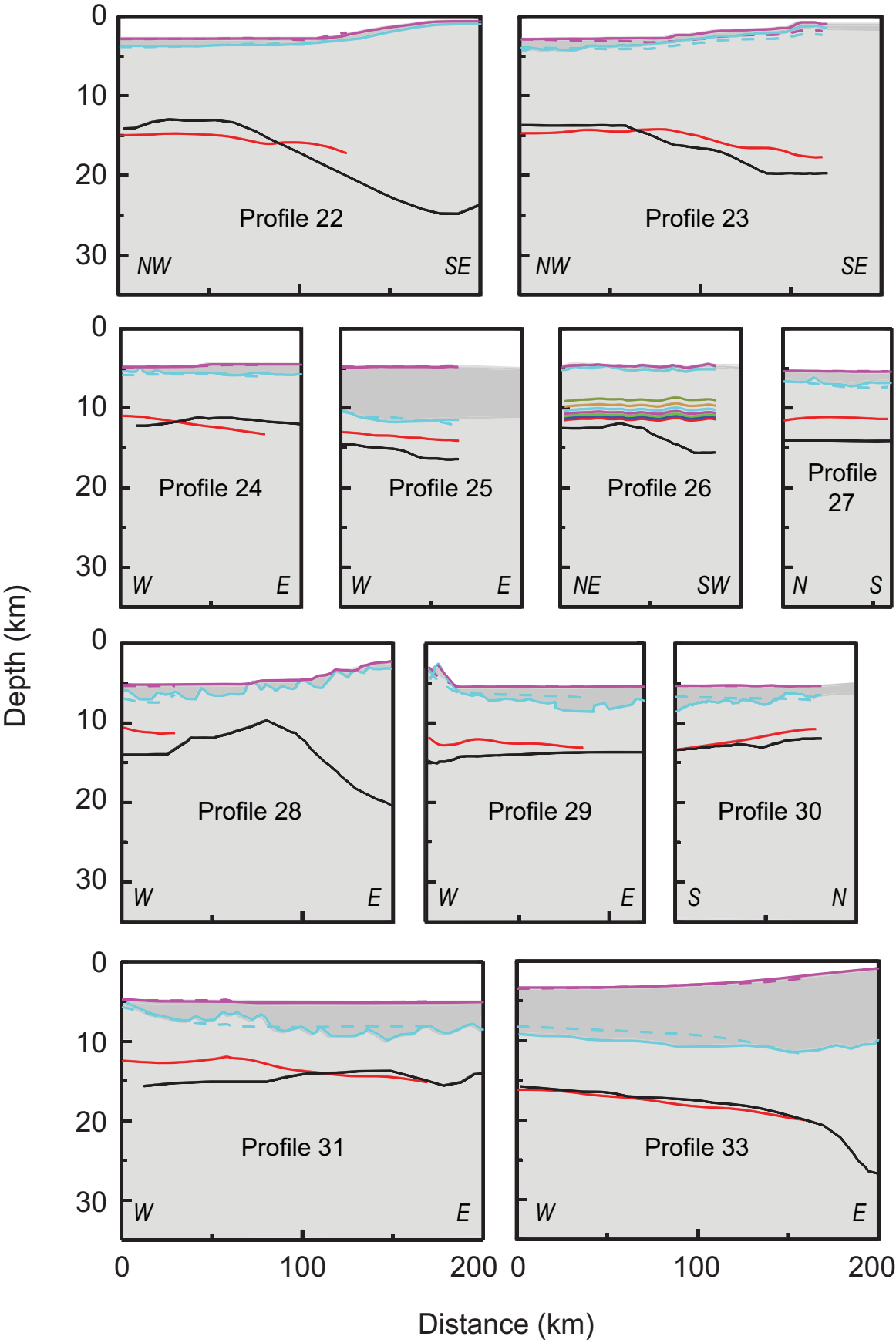
Depth (km)
0
10
20
30
Profile 22
NW
SE
Profile 23
NW
SE
Profile 24
W
E
Profile 25
W
E
Profile 26
NE
SW
Profile 27
N
S
Profile 28
W
E
Profile 29
W
E
Profile 30
S
N
Profile 31
W
E
Profile 33
W
E
0
100
200
Distance (km)

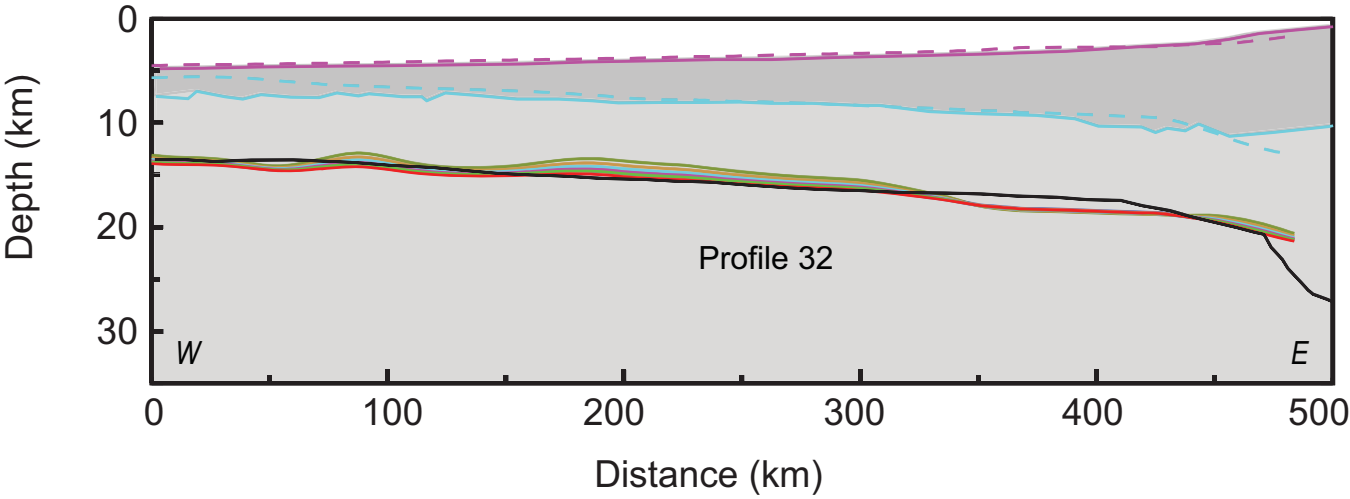
Depth (km)
0
10
20
30
Profile 32
W
E
0
100
200
300
400
500
Distance (km)